The Role of Interactions between Cucurbit[7]uril and Small Molecules in the Sodium Deoxycholate Hydrogel

by

Nikou Rahbari Asr

B.Sc, Sharif University of Technology, 2016

M.Sc, University of Victoria, 2024

A Thesis Submitted in Partial Fulfillment
of the Requirements for the Degree of

MASTER OF SCIENCE

in the Department of Chemistry

University of Victoria

Supervisory Committee

The Role of Interactions between Cucurbit[7]uril and Small Molecules in the Sodium Deoxycholate Hydrogel

by

Nikou Rahbari Asr

Bachelor of Science, Sharif University of Technology, 2016

Master of Science, University of Victoria, 2024

Supervisory Committee

Dr. Cornelia Bohne (Department of Chemistry)
Supervisor

Dr. David Leitch (Department of Chemistry)
Departmental Member

Dr. Stephanie Willerth (Department of Mechanical Engineering)
Outside Member

Abstract

The structure of bile salts has hydrophilic (hydroxyl groups) and hydrophobic (alkyl groups) regions, resulting in amphiphilic properties. Bile salts can form aggregates and these aggregates can act as supramolecular hosts for small molecules and encapsulate guest molecules within their structure. Unlike other bile salts, sodium deoxycholate (NaDC), can form supramolecular hydrogels through molecular self-assembly processes by adjusting the pH to around neutral and controlling the temperature.

The aim of this work, was to investigate how cucurbit[7]uril (CB[7]), affects the properties of NaDC hydrogel. Cucurbit[*n*]urils (CB[*n*]s) are a family of macrocyclic molecules characterized by their pumpkin-shaped structure and a symmetrical hydrophobic cavity. By studying the interactions of CB[7] in NaDC hydrogels, the aim was to understand the potential role of CB[7] in modifying the hydrogel's properties and to determine if CB[7] can serve as a carrier for guest molecules from the NaDC hydrogel to the surrounding medium. To gain a better understanding of the effect of CB[7] and its localization within the NaDC gel, two projects were developed.

The objective of the first project was to study how the presence of NaDC aggregates affects the binding dynamics of berberine, a natural isoquinoline alkaloid fluorophore, with the host CB[7] in the presence of mobile aggregates of the NaDC. The presence of NaDC aggregates creates a more heterogeneous environment for the host-guest interactions, potentially affecting the dissociation of berberine from CB[7]. The results showed that the addition of NaDC aggregates changed the distribution of berberine, causing berberine to bind to both CB[7] and NaDC aggregates. The results also revealed that the addition of NaDC aggregates to the berberine@CB[7] complex accelerated the apparent dissociation rate constant of berberine from CB[7].

The objective of the second project was to understand how the presence of CB[7] affects the structure of the NaDC hydrogel and the release of a small molecule from the hydrogel into the surrounding medium, and how this effect differs from the effect of cucurbit[6]uril (CB[6]). To study these effects, I studied the hydrogel's structure using berberine, a hydrophobic and positively charged guest, and rhodamine 6G, a hydrophilic and positively charged dye. The release of rhodamine 6G from the NaDC hydrogel into the surrounding medium was also studied in the presence of CB[7] and CB[6]. The results showed that the presence of CB[7] in the NaDC hydrogel caused the transformation of the spherical aggregates into elongated structures, whereas CB[6] led

to the formation of fibrous structures, as observed in previous research conducted by our group. Also, the release profile of rhodamine 6G from the NaDC hydrogel was not significantly affected by the addition of either CB[6] or CB[7].

Table of Contents

Supervisory Committee ii

Abstract iii

Table of Contents .....

List of Figures iv

List of Tables, Charts, Schemes x

List of Equations xi

List of Abbreviations xii

Acknowledgements xv

Dedication xvi

Chapter 1: Introduction 2

1.1. Supramolecular chemistry 2

1.2. Self-assembled and host-guest systems 4

1.3. Gels 5

1.3.1. Hydrogels 7

1.3.2. Mechanical properties and viscoelasticity of supramolecular hydrogels 9

1.4. Bile salts 10

1.4.1. Bile salts as hosts for small molecules 11

1.4.2. NaDC supramolecular hydrogel 12

1.4.3. Effect of additives on the properties and function of supramolecular hydrogels 12

1.4.4. Cucurbit[*n*]urils 13

1.5. Techniques 13

1.5.1. Absorption spectroscopy.....13

1.5.2. Fluorescence-based techniques.....14

1.5.2.1. Steady-state fluorescence.....15

1.5.2.2. Stopped-flow fluorescence technique.....16

1.5.2.3. Fluorescence microscopy.....17

1.6. Objective.....18

1.7. References.....19

Chapter 2 : Effect of sodium deoxycholate on the dissociation process of berberine cation from cucurbit[7]uril.....22

2.1. Introduction.....22

2.1.1. Cucurbit[*n*]uril chemistry.....22

2.1.2. Effect of metal ions on the binding kinetics of CB[*n*]s with guests.....23

2.1.3. Sodium deoxycholate.....23

2.1.4. Fluorescent probes: binding, photophysical properties, and applications.....25

2.1.4.1. Berberine as a fluorescence probe.....25

2.1.5. Objective.....26

2.2. Experimental Section.....27

2.2.1. Materials.....27

2.2.2. Sample preparation.....27

2.2.3. Instrumentation.....28

2.2.4. Data analysis for stopped-flow experiments.....28

2.2.5. Checking for the purity of berberine.....29

2.3. Results.....30

2.3.1. Absorption and steady-state fluorescence measurements.....30

2.3.1.1. Effect of the addition of NaDC on the berberine steady-state fluorescence and absorption spectra 30

2.3.1.2. Optimization of the excitation wavelength for berberine after binding to CB[7] and NaDC 32

2.3.1.3. Effect of CB[7] on the absorption spectrum of berberine.....37

2.3.1.4. Relocation of berberine with the addition of NaDC from the berberine@CB[7] complex.....37

2.3.1.5. Effect of addition of Ada^+ on the berberine fluorescence when berberine is bound to NaDC 39

2.3.2. Kinetic measurements.....41

2.3.2.1. Analysis of the displacement kinetics of berberine from the complex with CB[7].. 41

2.3.2.2. Determination of the association of berberine with NaDC aggregates.....42

2.3.2.3. Effect of Ada^+ addition on the berberine dissociation from the berberine@CB[7] complex in the presence of NaDC 43

2.3.2.4. Effect of the addition of NaDC on the displacement kinetics of berberine by Ada^+ from the berberine@CB[7] complex 44

2.4. Discussion.....47

2.5. Conclusion 52

2.6. References.....53

Chapter 3: Characterization of NaDC hydrogels after the addition of CB[7] by fluorescence microscopy and release studies.....55

3.1. Introduction.....55

3.1.1. Objective.....57

3.2. Experimental section....58
3.2.1. Materials....58
3.2.2. Sample preparation....58
3.2.3. Instrumentation....59
3.2.3.1. CLSM experiments....59
3.2.3.2. Release experiments by steady-state fluorescence....60
3.2.4. Effect of CB[6] on the morphology of the NaDC hydrogel....61
3.3. Results....63
3.3.1. Optimizing the CB[7] concentration for NaDC hydrogel formation....63
3.3.2 CLSM images of dyes with an NaDC/CB[7] ratio of 0.11....63
3.3.3. Confocal images of dyes with NaDC/CB[7] ratio of 0.15....66
3.3.4. Release studies....68
3.4. Discussion....70
3.5. Conclusion....73
3.6. References....74
Chapter 4: Summary....75
Appendix....78

List of Figures

Figure 1.1. Stimulation of observed rate constant of the binding of HSP^+ to CB[6] in the presence of different [Na^+]. Reprinted with permission from Bohne's work.[4] Copyright (2020) American Chemical Society. 3

Figure 1.2. Different types of gels. 6

Figure 1.3. Comparison of the hydrogels and organogels. 7

Figure 1.4. Schematic representation of stopped-flow fluorescence. 16

Figure 1.5. Schematic representation of a confocal laser scanning fluorescence microscope. 17

Figure 2.1. (a) Normalized steady-state fluorescence emission spectra of 30 μM berberine (λ_{ex} = 280 nm (black), 345 nm (blue), 400 nm (red)) in methanol. (b) Normalized steady-state fluorescence excitation spectra of 30 μM berberine in methanol normalized at 450 nm collected at different emission wavelengths (λ_{em} = 490 nm (black), 500 nm (blue), 650 nm (red)). 29

Figure 2.2. (a) Steady-state fluorescence emission spectra of 0.25 μM berberine (λ_{ex} = 345 nm) with (0, 1, 4, 6, 8, 10 mM) NaDC shown as a blue gradient (from light blue to violet) and (15, 20, 30, 50 mM) NaDC in red gradient (from pink to black). (b) Normalized steady-state fluorescence emission spectra of 0.25 μM berberine (λ_{ex} = 345 nm) with increasing NaDC concentrations shown in panel (a). (c, d) Fluorescence emission intensity at 550 nm for different concentrations of NaDC for two independent experiments. The plot shown in panel (c) is derived from data in panel (a) and panel (d) is derived from the data shown in the appendix (Figure A2.1). 30

Figure 2.3. Absorption spectra of 10 μM berberine in the absence (a, blue) and presence of 1, 4, 8, 20, 50 mM (b–f) NaDC ([Na^+] = 50 mM). 31

Figure 2.4. Steady-state fluorescence emission spectra of 0.25 μM berberine with an excitation wavelength of (a) 345 nm and (b) 420 nm with 5 (black), 10 (blue), 15 (red), 25 mM (green) NaDC ([Na^+] = 50 mM). 32

Figure 2.5. (a) Normalized steady-state fluorescence emission spectra of 0.25 μM berberine with an excitation wavelength of (a) 345 nm and (b) 420 nm, with 5 (black), 10 (blue),15 (red), 25 mM (green) NaDC ([Na^+] = 50 mM). 32

Figure 2.6. Normalized steady-state fluorescence emission spectra of 0.25 μM berberine (λ_{ex} = 345 nm, black; 420 nm, blue) with 5 (a), 10 (b), 15 mM (c) NaDC ([Na^+] = 50 mM). 33

Figure 2.7. Steady-state fluorescence emission spectra of 10 μM berberine with an excitation wavelength of (a) 345 nm and (b) 420 nm with 1 (blue), 5 (red), 10 (green), 30 μM (black) CB[7].....34

Figure 2.8. Normalized steady-state fluorescence emission spectra of 10 μM berberine (λ_{ex} = 345 nm) with 0 (black), 5 (blue), 20 (red), 30 μM (green) CB[7]. Spectra for 5, 20, 30 μM CB[7] are overlapping. The low signal to noise ratio in the spectrum of berberine with 0 μM CB[7] is attributed to the low emission quantum yield of free berberine in water 35

Figure 2.9. Plot for the dependence of the steady-state fluorescence 10 μM berberine (λ_{ex} = 345 nm) bound to different concentrations of CB[7], normalized to the emission at 500 nm of the highest concentration of CB[7].....36

Figure 2.10. Absorption spectra of 10 μM berberine with 0 (black), 1 (red), 10 (blue), 30 μM (green) CB[7] ([Na^+] = 50 mM). 37

Figure 2.11. (a) Steady-state fluorescence emission spectra of 0.25 μM berberine (λ_{ex} = 345 nm) and 0.75 μM CB[7] in the absence (black) and presence of low concentrations (1, 4, 6 mM) of NaDC shown as a red gradient from dark red to pink, and higher concentrations (8, 10, 15, 30, 50 mM) of NaDC shown as a blue gradient from purple to light blue. (b) Fluorescence intensities of the 0.25 μM berberine (λ_{ex} = 345 nm) and 0.75 μM CB[7] solution with different NaDC concentrations at 510 nm (black) and 550 nm (blue). The intensities were normalized to the intensity of berberine@CB[7]. (c) Dependence of the maximum emission wavelength of berberine@CB[7] on the NaDC concentrations. (d) Normalized spectra for the emission of berberine@CB[7] at different NaDC

concentrations. The data for panels (b),(c) and (d) were derived from the data in panel (a) 38

Figure 2.12. Steady-state fluorescence emission spectra of 0.25 μM berberine (λ_{ex} = 345 nm) with 25 mM NaDC with 0 (black), 40 (blue), 80 μM (red) Ada^+ ($[Na^+]$ = 50 mM) 40

Figure 2.13. Kinetic traces (black) for the mixing of a solution containing 5 μM Ada^+ with a solution containing of 0.25 μM berberine, 0.75 μM CB[7] and (a) 0 , (b) 25 mM NaDC ($[Na^+]$ = 50 mM). The fit of the experimental data to a monoexponential function is shown in blue and the residual between the experimental data and the fits are shown in the lower panels. All the concentrations mentioned are after mixing.....41

Figure 2.14. (a) Stopped-flow kinetic traces for the mixing of 0.25 μM berberine to 0 (black), 2 (blue), 15 (green), 25 mM (upper red) NaDC over a time scale of 2 s. (b) Stopped-flow kinetic traces for the mixing of 0.25 μM berberine in the absence (black) and presence (red) of 25 mM NaDC over a time scale of 0.025 s ($[Na^+]$= 50 mM). 42

Figure 2.15. (a) Stopped-flow kinetic traces for the mixing of the solution containing 0.25 μM berberine, 0.75 μM CB[7] and 25 mM NaDC with 2 (a, lower black), 5 (b, lower blue), 10 (c, red), 20 (d, green), 40 (e, upper black), 80 μM (f, upper blue) Ada^+ ($[Na^+]$ = 50 mM). All the concentrations mentioned are after mixing. Some of the traces are overlayed. (b) Averaged k_{obs} values for two independent experiments obtained by fitting the data using a monoexponential decay function. The k_{obs} values correspond the apparent dissociation rate constant (k_{-app}) values. The values shown are averages for the values obtained from the data in panel (a) and from Figure A2.2 in the appendix. 43

Figure 2.16. (a) Stopped-flow kinetic traces for the mixing of 5 μM Ada^+ with solutions containing 0.25 μM berberine, 0.75 μM CB[7] and different concentrations of NaDC. Lower concentrations of NaDC (0, 0.5, 2 mM) are shown as a blue gradient from light blue to purple and higher concentrations (5, 6, 15, 25 mM) are shown as a red gradient from pink to black ($[Na^+]$ = 50 mM). All concentrations mentioned are after mixing. (b) Averaged k_{obs} values from independent experiments obtained by fitting the data (panel (a)

and appendix A 2.3) using a monoexponential decay function. Error bars that are not visible are smaller than the data point shown. (c) Amplitudes for traces in panel (a). 44

Figure 2.17. (a) Stopped-flow kinetic traces for the mixing of 40 μM Ada^+ with the solutions containing 0.25 μM berberine, 0.75 μM CB[7] and different concentrations of NaDC. Low concentrations of NaDC (0, 2, 5, 10, 12 mM) are shown as a red gradient from black to light pink and higher concentrations (15, 20, 25 mM) are shown as a blue gradient from light purple to blue ($[Na^+]$= 50 mM). All concentrations mentioned are for after mixing. (b) Averaged k_{obs} values from two independent experiments panel (a) and Figure A 2.4 obtained by fitting the data using a monoexponential decay function. Errors bars that are not visible are smaller than the data point shown. (c) Amplitudes for traces in panel (a). 45

Figure 2.18. (a) Stopped-flow traces for the mixing of 80 μM Ada^+ with the solutions containing 0.25 μM berberine, 0.75 μM CB[7] and different concentrations of NaDC. Lower concentrations of NaDC (0, 2, 5, 10, 12 mM) are in red gradient from black to light pink and higher concentrations (15, 20, 25 mM) are in blue gradient from light purple to blue ($[Na^+]$ = 50 mM). All the concentrations mentioned are for after mixing. (b) k_{obs} obtained by fitting the data using a monoexponential decay function derived from data in panel (a). (c) Amplitudes for the traces in panel (a). Error bars are smaller than the data points shown. 46

Figure 3.1. Release profiles for pyrene (5 μM, left) and for rhodamine 6G (10 μM, right) dyes from NaDC gels (50 mM) with different CB[6]/NaDC ratios: 0 (red), 0.05 (blue), 0.1 (green), 0.15 (black). Reprinted with permission from [Sree Gayathri Talluri, Effect of cucurbit[6]uril on the structure and dynamics of NaDC gels, University of Victoria, 2021].[7] 56

Figure 3.2. Confocal images of CB[6]/NaDC with a ratio of 0.15 gel tagged with rhodamine 6G. Right and left panels correspond to the same sample. 61

Figure 3.3. NaDC/CB[7] hydrogels with NaDC/CB[7] ratios of (a) 0.15 (b) 0.12 (c) 0.11.. 63

Figure 3.4. Confocal images of NaDC/CB[7] gel tagged with rhodamine 6G at an CB[7]/NaDC ratio of 0.11. All panels correspond to a same sample. 64

Figure 3.5. Confocal images of NaDC/CB[7] gel tagged with berberine at CB[7]/NaDC ratio of 0.11 in different depths (Z = 102–302 μm) of hydrogel. The scale bars correspond to 20 μm. 65

Figure 3.6. Confocal images of NaDC/CB[7] gel tagged with rhodamine 6G at CB[7]/NaDC ratio of 0.15. Both panels correspond to a same sample. 66

Figure 3.7. Confocal images of NaDC/CB[7] gels tagged with berberine at CB[7]/NaDC ratio of 0.15 ([NaDC] = 50 mM). All panels correspond to a same sample. 67

Figure 3.8. Confocal images of NaDC/CB[7] gel tagged with berberine at CB[7]/NaDC ratio of 0.15 in different depth (Z = 54–234 μm) of hydrogel. The scale bars correspond to 20 μM.....67

Figure 3.9. (a) Steady-state fluorescence emission spectra of known concentrations of rhodamine 6G (λ_{ex} = 480 nm) in phosphate buffer used to establish the calibration curve. (b) Calibration curve derived from the data in panel (a). 68

Figure 3.10. (a) Steady-state fluorescence emission spectra of the surrounding medium collected at different times during the release of 10 μM rhodamine 6G (λ_{ex} = 480 nm) from (a) NaDC/CB[6] ([NaDC] = 50 mM, CB[6] = 5 mM) and (b) NaDC/CB[7] ([NaDC] = 50 mM, CB[7] = 5 mM) hydrogels. Data was obtained between 0–330 min. 69

Figure 3.11. Release profile of 10 μM rhodamine 6G from (a) NaDC/CB[6] ([NaDC] = 50 mM, [CB[6]] = 5 mM, circle,black) and (b) NaDC/CB[7] ([NaDC] = 50 mM, [CB[7]] = 5 mM, square, blue) hydrogels. Lines are drawn to guide the eye. 70

Figure 4.1. Schematic representation of the connection between supramolecular systems' structure, thermodynamics, and dynamics. 75

Figure A2.1. Steady-state fluorescence emission spectra of 10 μM berberine (λ_{ex} = 345 nm) with 1 (a, lower black), 5 (b, lower blue), 10 (c, lower red), 15 (d, green), 20 (e, upper blue), 30 (f, upper black), 50 mM (upper red) (a → g) NaDC. 78

Figure A2.2. Stopped-flow kinetic traces for the mixing of a solution containing of 0.25 μM berberine with 0.75 μM CB[7] and 25 mM NaDC with 2 (black), 5 (lower blue), 10 (red), 20 (lower green), 40 (black), 80 μM (upper green) Ada^+ ($[Na^+]$ = 50 mM). All the concentrations mentioned are after mixing. All traces except the green trace are overlapping. 78

Figure A2.3. Stopped-flow kinetic traces for the mixing of 5 μM Ada^+ with solutions containing 0.25 μM berberine, 0.75 μM CB[7] and different concentrations of NaDC. Lower concentrations of NaDC (0, 0.5, 2 mM) are shown as a blue gradient from light blue to purple and higher concentrations (5, 6, 15, 25 mM) are shown as a red gradient from pink to black) ($[Na^+]$ = 50 mM). All the concentrations mentioned are after mixing. 79

Figure A2.4. Stopped-flow kinetic traces for the mixing 40 μM Ada^+ with solutions containing 0.25 μM berberine, 0.75 μM CB[7] and different concentrations of NaDC. Low concentrations of NaDC (0, 2, 5, 10, 12 mM) are shown as a red gradient from black to light pink and higher concentrations (15, 20, 25 mM) are shown as a blue gradient from light purple to blue ($[Na^+]$ = 50 mM). All the concentrations mentioned are for after mixing. 79

List of Tables, Charts, Schemes

Scheme 1.1. A schematic representation of the antigen-antibody interaction. 2

Table 1.1. Classification of hydrogels based on the nature of the interactions between building blocks.....8

Scheme 1.2. Schematic representation of the micellization in water. 9

Chart 1.1. Molecular structures of bile salts including: (a) NaDC, (b) NaTDC, (c) NaTC, (d) NaCh.....10

Chart 1.2. Molecular structure of CB[*n*]s 13

Chart 2.1. Molecular structures of (a) CB[7] and (b) Ada^+ cation. 22

Chart 2.2. Molecular structure of NaDC. 23

Scheme 2.1. Schematic representation of the formation of NaDC primary (b) and secondary (c) aggregates from NaDC monomers (a). Reprinted and modified with permission from Bohne's work. Copyright (2009) American Chemical Society.....24

Chart 2.3. Molecular structure of berberine chloride. 25

Chart 3.1. (a) Chemical structure of rhodamine 6G. (b) Chemical structure of pyrene. ..57

Scheme 3.1. Schematic representation of the static diffusion method for release studies 60

List of Equations

Equation 1.1.....14
Equation 2.1.....23
Equation 2.2.....28
Equation 2.3.....49
Equation 2.4.....49
Equation 2.5.....49
Equation 2.6.....49
Equation 2.7.....49

List of Abbreviations

2D	Two dimensional
3D	Three dimensional
Å	Ångstrom
A	Absorbance
Ada	Adamantane
Ada^+	Adamantylammonium cation
AU	Airy unit
°C	Degree Celsius
C	Concentration of absorbing species
CB[*n*]	Cucurbit[*n*]uril
CB[6]	Cucurbit[*6*]uril
CB[7]	Cucurbit[*7*]uril
CLSM	Confocal laser scanning microscopy
cm	Centimeter
DNA	Deoxyribonucleic acid
ΔG	Change in Gibbs free energy
ΔH	Change in enthalpy
ΔS	Change in entropy
λ_{ex}	Excitation wavelength
λ_{em}	Emission wavelength
ε	Molar absorptivity
G’	Storage modulus

G”	Loss modulus
h	Hour
HSP^+	Trans-1-methyl-4-(4-hydroxystyryl)pyridinium cation
I_0	Intensity of the incident light
I	Intensity of the light after passing through the sample
IR	Infrared
K_{eq}	Equilibrium constant
k_{-app}	Apparent dissociation rate constant
k_+	Association rate constant
k-	Dissociation rate constant
k_{obs}	Observed rate constant
LMWG	Low molecular weight gelator
LWD	Long working distance
LSM	Laser scanning microscope
min	Minute
mL	Millilitre
mM	Millimolar
mmol	Millimoles
μM	Micromolar
μL	Microlitre
Na^+	Sodium ion
NaCl	Sodium chloride
NaDC	Sodium deoxycholate

NaH_2PO_4	Monosodium phosphate
Na_2HPO_4	Disodium phosphate
NaTC	Sodium taurocholate
NaTDC	Sodium taurodeoxycholate
nm	Nanometer
NMR	Nuclear magnetic resonance
pH	Potential of hydrogen
RNA	Ribonucleic acid
s	Second
T	Temperature
UV-Vis	Ultraviolet-Visible
V	Voltage

Acknowledgements

I would like to express my deepest gratitude to my supervisor Dr. Cornelia Bohne, for her invaluable guidance, support, and encouragement throughout my research journey. Her expertise and mentorship have been instrumental in shaping my academic growth and the completion of this thesis.

I also wish to thank my lab mates, Gustavo Lopes Camelo, Dr. Ankur Awasthi, Dr. Sree Gayatri Talluri, Dr. Karina Argüello, Guanqiao Wang and Victor Toledo for their collaboration, and the stimulating discussions that made our lab a vibrant place for research. A special thanks to Luis Netter for his assistance with technical issues in the lab; his expertise and willingness to help were greatly appreciated. I would also like to extend my sincere thanks to Dr. Stanislav Konorov for his training on microscopy and for patiently addressing my questions throughout my studies. A special mention goes to Jessy Oake, our research assistant, for her dual role in providing support in both research and training. Her guidance and assistance were invaluable. Moreover, her emotional support and willingness to lend an ear whenever I needed someone to talk. Her empathy and understanding were crucial in helping me overcome both academic and personal challenges. I am deeply grateful to Dr. Behzad Pourbadiei, my undergraduate supervisor, for his encouragement and support, which played a key role in my decision to pursue graduate studies.

Special thanks go to my friends in Canada—Sara, Afsane, and Yasaman—for their emotional support. Their friendship and encouragement were crucial in helping me navigate the challenges of this journey.

I extend my heartfelt thanks to my family for their unwavering love and support. Their belief in me has been a constant source of strength and motivation. This work would not have been possible without their sacrifices and understanding.

Finally, I would like to express my appreciation to the NSERC CREATE PoND program, NSERC, CAMTEC, and UVic for their financial and technical support throughout my studies.

Dedication

My mom, dad and sister

Chapter 1: Introduction

1.1. Supramolecular chemistry

Supramolecular chemistry is the study of the interactions between molecules that are held together by non-covalent forces, leading to a system. Supramolecular chemistry studies weak and reversible interactions between molecules, in contrast to molecular chemistry, which is largely concerned with the study of covalent bonds of molecules. Non-covalent interactions including hydrogen bonding, metal-ion coordination, π-π stacking, and the hydrophobic effect are reversible, giving the supramolecular system a dynamic behavior.[1] This reversible binding is essential for different applications, in fields like drug delivery[2] and molecular sensors.[3] Similarly, in biological systems, non-covalent and reversible interactions play a critical role in many processes.

In fact, biological systems, such as the structures of proteins, DNA, and RNA, served as early inspirations for the study of supramolecular complexes. Complex formation by weak intermolecular forces plays important roles in many interactions within the body, such as those occurring in the cell membrane. For example, binding between antibodies and antigens which is the main fundamental response of the immune system, is mostly by binding of the antigen to the unique binding site on the structure of the antibody (Scheme 1.1) leading to a defense mechanism. The ability of supramolecular systems to form specific 3-D structures is comparable to the complex molecular interactions found in biological systems.

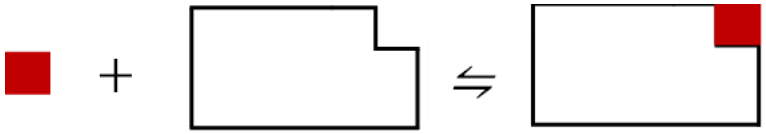

Scheme 1.1. A schematic representation of the antigen-antibody interaction.

When a single component is added to a supramolecular system, it can interact in a specific way with the existing molecules, leading to a particular behavior of the whole system. However, when more than one component is added, the interactions may become more complex. The additional molecules could interact with one another as well as with the existing molecules, forming new and different interactions that can change the overall behavior of the system. This complexity can lead to a different behavior than what was observed with just the single component.

For instance, the binding dynamics between the *trans*-1-methyl-4-(4-hydroxystyryl)pyridinium cation (HSP^+) and cucurbit[6]uril (CB[6]) were investigated in the presence of different concentrations of sodium cations (Na^+). The analysis and interpretation of the results showed that the addition of Na^+ led to the changing of the dynamics of the system.[4]

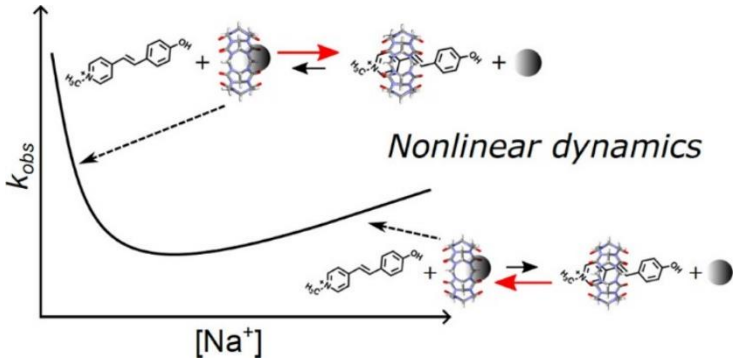

Figure 1.1. Simulation of observed rate constant of the binding of HSP^+ to CB[6] in the presence of different [Na^+]. Reprinted with permission from Bohne's work.[4] Copyright (2020) American Chemical Society.

Figure 1.1 shows the simulation for the effect of changing Na^+ concentration on the observed rate constant (k_{obs}) for the binding of the guest molecule (HSP^+) with CB[6]. CB[6] binds to Na^+ through the carbonyl portals of CB[6], which can change the rate constant of binding of guest molecules to CB[6]. Interestingly, as the Na^+ concentration increases, there is a non-linear change in the trend of the observed rate constants. The observed rate constant decreases as the Na^+ concentration continues to rise until a certain point. After this point, as the concentration of Na^+ increases further, the k_{obs} starts to increase. This change in k_{obs} from low to high concentrations of Na^+ is not linear. Non-linearity in the observed rate constant in different Na^+ concentration ranges highlights the complexity of competitive binding between guest molecules with a host binding site, emphasizing the challenges of predicting such interactions.[4] Because, the binding of one guest molecule can influence the binding of others and hence, complicating the overall binding behavior.

The mechanisms of the interactions in supramolecular systems are poorly understood, unlike the well-defined covalent bonds in molecular systems. For this reason, parameters

involved in the formation of a specific supramolecular system (product) from individual molecules (reagents) are not clear.[1]

The long-term objective of studying supramolecular systems is to replicate the functional diversity observed in living organisms. Overcoming the current lack of knowledge between the potential supramolecular assemblies requires a deep understanding of how molecules in biological systems self-assemble.[5] Understanding the interrelationships between the dynamics, thermodynamics, and structure of the system is essential for advancing the field of supramolecular systems.

1.2. Self-assembled and host-guest systems

Supramolecular systems can be broadly divided as either host-guest systems or self-assembled systems. Division of the supramolecular systems into host-guest and self-assembled systems are based on the structural organization of the molecules involved. Self-assembly is the spontaneous assembly of molecules into well-defined structures. Self-assembly occurs through the recognition and pairing of complementary counterparts in a mixture, a phenomenon known as self-sorting. For a process to occur spontaneously, ΔG must be negative. A negative ΔG can happen in two ways: when ΔH is negative, along with an exothermic release of heat, and when $T\Delta S$ is positive, indicating that a positive ΔH is overcome by the increase in entropy. Even an endothermic reaction (positive ΔH) can proceed spontaneously if the increase in entropy is significant enough to make $T\Delta S$ larger than ΔH. In a self-assembled system, the transition from disorganization to organized assembly is often driven by thermodynamic forces. While the local organization of molecules may lead to a decrease in entropy, the overall system can experience an increase in entropy due to the release of solvent molecules. Self-assembled structures, such as aggregates and micelles, form through intermolecular interactions. Micelles show an increase in overall entropy, as their formation releases water molecules from the hydrophobic parts into the surrounding solution, thus increasing the system's entropy.

Another type of supramolecular systems are host-guest systems which involve the accommodation of a smaller molecule (guest molecule) within the cavity or binding to the binding site of another molecule (host molecule). Cyclodextrins, cucurbiturils, and calixarenes are well-known examples of host molecules. The specificity and strength of host-guest interactions depend on factors such as the size, shape, charge, and functional groups of both the host and guest molecules.[7] For example, Stella and colleagues studied how the presence of charge affects the binding affinity between cyclodextrins and guests. Their findings showed that neutral molecules showed a stronger interaction with anionically charged cyclodextrins in comparison to neutral cyclodextrins. Also, when the guests had a charge (either positive or negative), the complexes formed with neutral cyclodextrins showed a decrease in strength compared to the interactions involving the neutral forms of the same molecules.[8]

Supramolecular chemistry contains systems that bring together both self-assembly and host-guest interactions. These mixed systems involve molecules that can self-assemble into larger structures, such as micelles, and they contain host-guest interactions between specific molecules within the assembly. For example, a system that has amphiphilic molecules capable of self-assembly and host molecules that can interact with guest molecules. Amphiphilic molecules are compounds that contain both hydrophilic and hydrophobic regions within their structure. Amphiphilic molecules may form the basic structure through self-assembly, while the host molecules within this structure can selectively bind guest molecules. This combination of self-assembly and host-guest interactions adds complexity and functionality to the system.

1.3. Gels

Gels are three-dimensional networks that form when molecules self-assemble into a solid or semi solid state.[9] The unique properties and mechanical strength of gels are characterized by the self-assembled structures they form, which can manifest as fibers, sheets, or clusters.
The structure of a gel can give mechanical strength, porosity, viscoelasticity, optical properties, biological and chemical reactivity.[10] Gels can be classified based on different criteria such as solvent, composition, origin, and structure. In one classification, gels can be broadly divided into solid and semi solid gels based on their physical properties and behavior (Figure 1.2).[11]

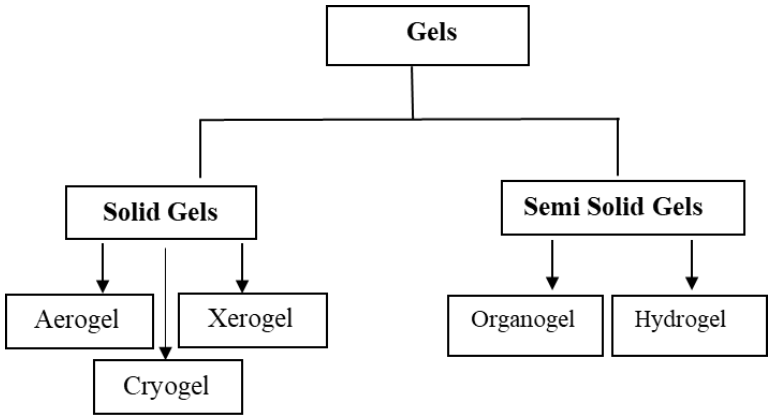

Figure 1.2. Different types of gels.

Aerogels, cryogels, and xerogels are porous materials with diverse properties and applications.[12] Aerogels are lightweight and excellent thermal insulators due to their high porosity and low density. The most common type of aerogels are silica aerogels. Cryogels are dried at very low temperatures, resulting in large pores suitable for rapid diffusion and applications requiring low thermal conductivity.[13] Xerogels, which are dried at ambient pressure, are denser than aerogels and cryogels due to some pore collapse. Semi solid gels, in contrast, contain a significant amount of solvent within their structure, giving them a softer structure that allows them to deform more easily under stress compared to solid gels. One classification of the semi solid gels is based on the type of solvent in the mobile phase of the gel (Figure 1.3). If the mobile phase of the gel is an organic solvent, the gel is classified as an organogel, whereas if the mobile phase is mostly water or other aqueous solvents, it is termed a hydrogel. The significant advantage of organogels is their broader selection of liquid phases. However, the primary disadvantage comes from their limited biocompatibility.[14]

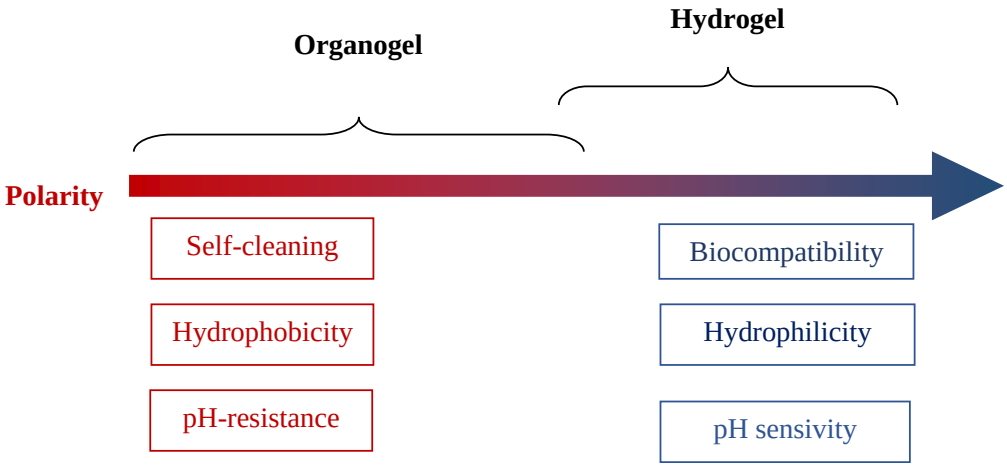

Figure 1.3. Comparison of the hydrogels and organogels.

Since their mobile phase is comprised of aqueous solvents, hydrogels have a higher polarity than organogels, which are predominantly less polar due to the presence of organic solvents. Hydrogels and organogels have different properties due to their distinct structural characteristics (Figure 1.3). Hydrogels generally have a higher pH-sensitivity, hydrophilicity, and biocompatibility compared to organogels. The swelling behavior of hydrogels arises from their high water content, causing them to be suitable for wound healing applications, tissue engineering scaffolds, and pH-triggered delivery systems.[15] For example, Kim and coworkers worked on a hydrogel, composed of a copolymer of *N*-isopropyl acrylamide and glycidyl methacrylate functionalized with melamine units that showed responsiveness to changes in pH, with significant drug release observed at pH 4.0.[16]

1.3.1. Hydrogels

Hydrogels are a category of gels that incorporate mostly water as their mobile phase. Hydrogels can shrink in response to specific conditions and external stimuli. The three-dimensional network in hydrogels is formed by the immobile phase, which consists of crosslinked polymers or other molecules within the hydrogel. This immobile phase of hydrogels is responsible for shaping the hydrogel and giving a semi solid nature to it.

Table 1.1. Classification of hydrogels based on the nature of the interactions between building blocks.

Hydrogels

CHEMICAL HYDROGELS	***PHYSICAL HYDROGELS***
Covalent bonding	Physical interactions
Mechanical strength is higher	Show reversibility
High molecular weight gelators	Low molecular weight gelators

Hydrogels can be classified into two main categories based on the interactions between the building blocks: chemical hydrogels and physical hydrogels (Table 1.1). If the interactions between the building blocks involve covalent bonds, the resulting hydrogel is termed a chemical hydrogel. The covalent bonds in the chemical hydrogels' 3-D network provide strength to the hydrogel. However, the non-reversibility of the covalent bonds limits their tunability for some applications.

Physical hydrogels are a class of hydrogels that form through reversible, and non-covalent interactions. Physical hydrogels can be formed through different methods, in processes such as crystallization, the aggregation of amphiphilic molecules, charge-charge interactions, hydrogen bonding, and interactions involving proteins.[17] Physical hydrogels could be smart which means that responding to environmental stimuli, making them suitable for applications where stimuli-triggered changes in the gel's properties are desired such as drug delivery[18], and tissue engineering.[19] For instance, chitosan microspheres that are sensitive to pH were incorporated into a thermoresponsive hydrogel to form a smart composite hydrogel and because of their electrostatic characteristics, they could bind and release salicylic acid as a model drug.[20]

Physical hydrogels are divided into two types: physical entanglements and low molecular weight gelators (LMWG). Physical entanglement hydrogels have polymeric gelators and possess both hydrophobic and hydrophilic segments within their structure, leading to the formation of micelles in specific conditions with high molecular weights. Micelles (Scheme 1.2), which are

formed by molecules with hydrophobic and hydrophilic segments, can aggregate at a critical micellization concentration. The entanglement of micelles can form physical hydrogels. In physical hydrogels, the hydrophobic core of the micelles is positioned on the inside, while the outer part consists of the hydrophilic portion of the micelles, which interacts with water.

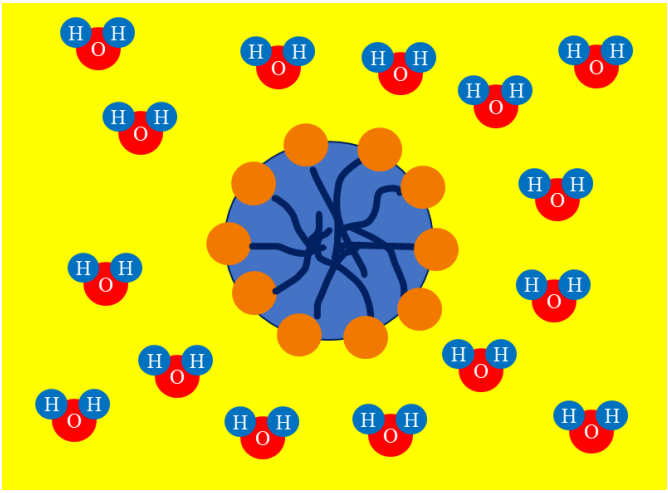

Scheme 1.2. Schematic representation of the micellization in water.

When the building blocks have lower molecular weight, they are classified as LMWG, forming supramolecular hydrogels.

1.3.2. Mechanical properties and viscoelasticity of supramolecular hydrogels

One of the aspects of supramolecular hydrogels is their low mechanical strength. Mechanical strength is the ability of the hydrogel's network of building blocks to withstand deformation under mechanical forces which can be studied by rheology. The mechanical strength is affected by the cross-linking density of the 3-D network and the nature of the molecular interactions within the hydrogel. Non-covalent interactions are easier to deform, especially when compared to polymeric hydrogels. Understanding the factors that affect the formation of supramolecular systems can help achieve a balance between bond reversibility and mechanical strength in these hydrogels. This balance can be achieved by modifying the building blocks within the hydrogels.

Supramolecular hydrogels show higher mechanical strength than liquids against mechanical forces while retaining liquid-like characteristics because of their viscoelastic

behaviour, which combines the characteristics of solids and liquids. In rheology, the viscoelastic properties of a hydrogel are characterized by the storage modulus (G') and the loss modulus (G"). G' measures the gel's ability to maintain its shape under stress, while G" is the energy dissipated when the gel is deformed. Typically, G' is higher than G", indicating solid-like behavior, in contrast to liquids where G" is higher. This difference in the G' and G" values in hydrogels distinguish them from liquids due to their viscoelastic nature.

1.4. Bile salts

Bile salts are steroids that have a key role in the body's fat absorption process. Bile salts serve as surfactants by solubilizing fats in aqueous media.[21] Amphilicity of the bile salts are due to the presence of both hydrophilic (hydroxyl groups) and hydrophilic (alkyl groups) parts within their structure. Sodium cholate (NaCh), sodium taurocholate (NaTC), sodium deoxytaurocholate (NaTDC), and sodium deoxycholate (NaDC) are different types of bile salts (Chart 1.1).

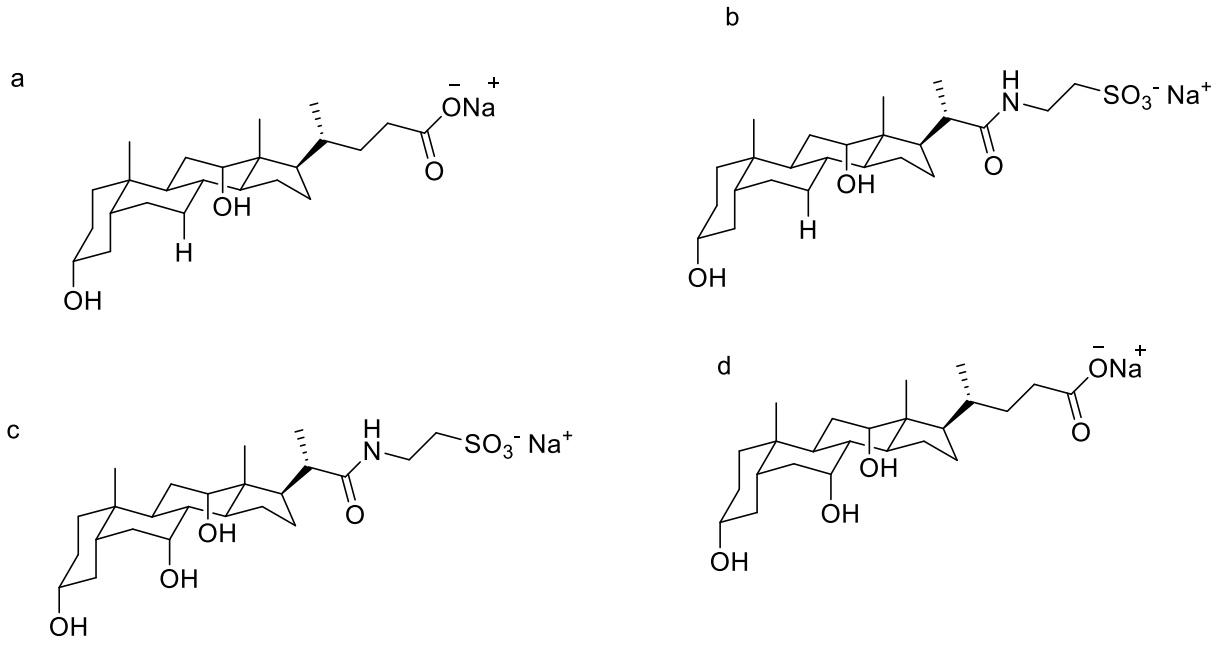

Chart 1.1. Molecular structures of bile salts including: (a) NaDC, (b) NaTDC, (c) NaTC, (d) NaCh.

The primary factors of structural differences between bile salts are the presence or absence of hydroxyl groups, and the conjugation with amino acids like taurine. These structural modifications affect properties of the bile salts such as their solubility.

1.4.1. Bile salts as hosts for small molecules

Due to the amphiphilic nature of the bile salts, they can form aggregates in a proper solvent. This aggregation is different from traditional micellization in the sense that, in micelles, one portion of the molecule is hydrophobic, and a tail hydrophilic group is present, which is not the case for bile salt aggregates. The process by which bile salts aggregates form larger structures is described by several models. In the more accepted model,[22] it was proposed that bile salts form two types of supramolecular aggregates. First, bile salts form primary aggregates (smaller aggregates). Primary aggregates have hydrophobic binding sites within their structure, and guests that are bound to the primary aggregates are well-protected from aqueous media. Pyrene, a hydrophobic and neutral guest, binds to the hydrophobic binding sites of the bile salt aggregates,[23] as indicated by its steady-state fluorescence, which is sensitive to the polarity of the environment.[24] By increasing the concentration of bile salts, some of the primary aggregates assemble into larger secondary aggregates. Secondary aggregates are more hydrophilic, and guests with higher hydrophilicity bind to the binding sites of secondary aggregates.[25-27]

The structures of the primary and secondary aggregates vary for each bile salt, and the binding of the small molecules to the aggregates of different bile salts also differs from one another based on the properties of both host (aggregates) and guest. There are some studies in the literature showing the connection between the properties and structures of guest molecules and the bile salt aggregates. For example, it has been suggested that the binding efficiency of guests to bile salts that form smaller aggregates, such as NaDC and NaTDC, is higher than the other bile salts. Also, the residence time of the guest molecules inside in the aggregates depends on the structure of the guest such as presence of short alkyl substituents in the guest structure.[28] Also, it was shown that the addition of a co-solvent, which results in changing the polarity, can affect the binding and residence time of the guests in bile salt aggregates.[29, 30]

1.4.2. NaDC supramolecular hydrogel

Among bile salts, NaDC aggregates can form a supramolecular hydrogel by acting as a LMWG.[31] Before gelation, NaDC molecules form mobile primary and secondary aggregates. These aggregates eventually interact and organize, leading to the formation of a stable NaDC hydrogel. A study showed that ionic interactions affect the formation of NaDC hydrogels. For instance, adjusting the pH, can change the properties of the NaDC hydrogels such as mechanical strength, sol-gel temperature, and crystallinity. By adjusting the pH to around neutral and controlling the temperature based on the concentration of NaDC, immobile aggregates start to form and create the gel network through physical interactions.[32] NMR studies have shown that more than half of the aggregates remain free in the aqueous phase after gelation, and the rest become immobilized in the 3-D gel network.[33] The main driving force that causes the formation of the NaDC hydrogel is hydrogen bonding.[34] During gelation, the complexity of the binding of the guests to NaDC aggregates increases, as there are more binding sites available for these molecules to bind. Hence, NaDC hydrogels create a supramolecular platform for small molecules to bind differently in various parts of the mobile and immobile phases. Earlier studies in Bohne group showed that adding pyrene to a freshly prepared NaDC hydrogel changes the polarity of the microenvironment of pyrene. Changing the polarity of the microenvironment around pyrene suggests an interaction between pyrene and the hydrophobic, immobilized NaDC aggregates.[35]

1.4.3. Effect of additives on the properties and function of supramolecular hydrogels

Different compounds can be added to supramolecular hydrogels as additives to change or improve the hydrogel's properties. For example, Guiying Xu and co-workers showed that addition of some of the amino acids such as *L*-lysine and *L*-arginine prevent gelation of the NaDC in room temperature as observed by microscopy, IR and rheological studies.[36] The disruption of hydrogen bonds, leads to the transition of the gel to a solution in the presence of these amino acids. In another study, it was shown that adding CB[6], increases the mechanical strength of the NaDC hydrogel.[35] CB[6] not only strengthens the NaDC gel but also changes the distribution of guests within the gel.[37]

1.4.4. Cucurbit[*n*]urils

Cucurbit[*n*]urils [CB[*n*]s], are macrocycles that have two portals lined with carbonyl groups, a hydrophobic cavity, and a symmetrical structure.[38] The carbonyl portals and cavity of CB[*n*]s can act as hosts for small molecules within the gel matrix. For instance, CB[6] was added to a NaDC hydrogel as an additive, interacting with pyrene and modifying its release profile.[35,39] The change in pyrene release from the gel to the surrounding medium occurred because pyrene can interact with both NaDC aggregates and CB[6]. Therefore, adding CB[6] changed the distribution of guest (pyrene) in the gel network. On the other hand, CB[6] can act as a guest and an additive inside the NaDC aggregates. This interaction between NaDC hydrogel and CB[6] changes the binding process between the guests and the binding sites within the supramolecular hydrogel.

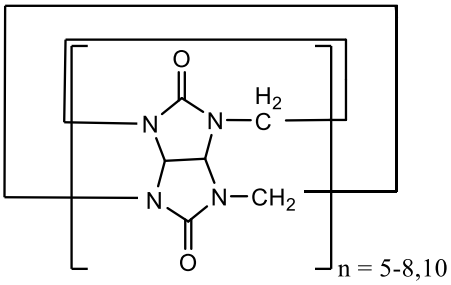

Chart 1.2. Molecular structure of CB[*n*]s.

1.5. Techniques

1.5.1. Absorption spectroscopy

Different molecules can absorb light at different wavelengths depending on the type of molecule and its structure. UV-VIS spectroscopy can be used to determine the wavelength of the absorbed light if it falls within the UV or visible regions of the electromagnetic field around 200 nm to 800 nm. In UV-VIS spectroscopy, the Beer-Lambert law is a basic concept that establishes a quantitative connection between a sample's concentration and light absorbance.

$$A = \varepsilon cl = \log\frac{I_0}{I}$$ **Equation 1.1**

Equation 1.1 shows Beer-Lambert law. In this equation, *A* is the absorbance of the sample, *ε* is the molar absorptivity, *c* is the concentration of the absorbing species in the sample, and *l* is the pathlength of the sample. By UV-VIS spectroscopy and this law, samples can be analyzed quantitatively. Light scattering is a major limitation of UV-Vis spectroscopy when analyzing gels. Gels often have non-uniform structures or particles that scatter incoming light, which causes deviations in absorbance readings.

UV-Vis absorption shows the ground state association of small molecules with NaDC aggregates, indicating that UV-Vis spectroscopy is used to analyze the interactions between these small molecules and NaDC aggregates when both are in their lowest energy state. For example, Han and coworkers showed the binding of ferulic acid with NaDC monomers, primary and secondary aggregates. Absorption and fluorescence measurements in this study showed that the interaction between folic acid and NaDC involves both hydrophobic forces and hydrogen bonding.[40]

1.5.2. Fluorescence-based techniques

Fluorescence-based techniques involve a characterization process where a molecule absorbs light at specific wavelengths and emits light at longer wavelengths. Valuable information into the interactions between the fluorophore and its surroundings can be obtained by examining the different fluorescence properties, including lifetime, intensity, and quenching. The advantage of fluorescence-based techniques compared to other spectroscopic techniques is their high sensitivity even at low concentrations of the dyes. Supramolecular hydrogels are formed by non-covalent interactions, and adding high concentrations of a dye could significantly change their properties. Therefore, fluorescence-based techniques are useful for studying supramolecular hydrogels, as they allow the properties of the gel to be studied without changing the gel's structure by adding only a small amount of dye.

1.5.2.1. Steady-state fluorescence

Steady-state fluorescence is a fluorescence method in which the compound is continuously excited by a light source, reaching its equilibrium state at a specific wavelength, typically the maximum absorption wavelength of the fluorophore. By determining the fluorescence intensity of a known concentration of an analyte, the amount of dye can be quantified. The relationship between fluorescence intensity and analyte concentration is typically linear within a specific range. As the concentration of the analyte increases, the number of excited fluorescent molecules also increases. This direct correlation between fluorescence intensity and analyte concentration allows for the quantification of the analyte.

Fluorescence measurements in different conditions help as a tool for studying molecular interactions, structural changes, and environmental effects on samples. By titrating a titrant into a solution, the binding isotherm can be obtained, providing information about the binding interactions. Fluorescence measurements at different pH values can give information about protonation/deprotonation processes. Also, changes in temperature during fluorescence studies can explain conformational changes and thermal stability of the reaction. Steady-state fluorescence can also help in the understanding of detailed characteristics of supramolecular systems, such as NaDC aggregates. For instance, quenching studies of pyrene in the presence of NaDC hydrogels were conducted to study the structure of the hydrogel.[37]

1.5.2.2. Stopped-flow fluorescence technique

The stopped-flow technique is a fluorescence method in which two or more reactants are rapidly mixed together, and the fluorescence of the reactants is monitored from the start of the reaction until the reaction reaches an equilibrium state.[41]

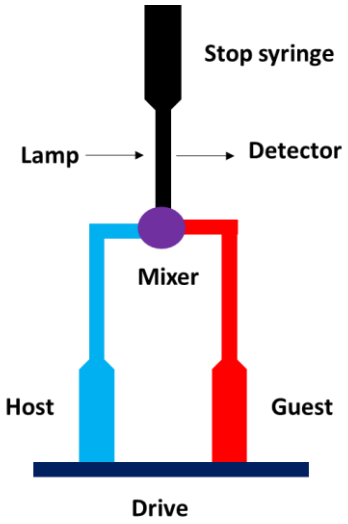

Figure 1.4. Schematic representation of stopped-flow fluorescence.

The main components of a typical stopped-flow instrumentation include two syringes, each containing a reactant, connected to a mixing chamber (Figure 1.4). This chamber has an observation cell for monitoring the reaction. A rapid mixing allows simultaneous injection of reactants into the observation cell, ensuring mixing within milliseconds. Detection of the reaction employs spectroscopic methods like absorbance or fluorescence spectroscopy, which are chosen based on the reactants and the nature of the reaction. This system enables the collection of time-resolved data, capturing kinetics of the reaction immediately after mixing. Researchers can analyze data from stopped-flow to obtain kinetic information, providing information about the mechanisms and kinetics of rapid chemical reactions. Some stopped-flow systems also have temperature control for studying temperature-dependent reaction kinetics.

1.5.2.3. Fluorescence microscopy

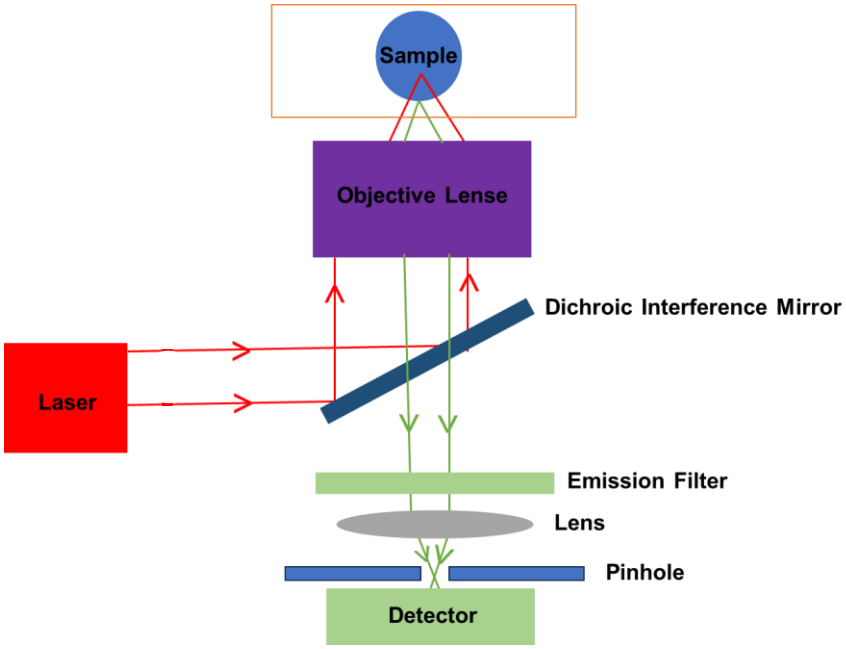

Figure 1.5. Schematic representation of a confocal laser scanning fluorescence microscope.

A confocal laser scanning fluorescence microscope (CLSM) is a type of optical microscope that uses fluorescent samples. A CLSM includes magnifying lenses, a dichroic mirror, and a filter. The dichroic mirror and the emission filter then select the emitted light from the sample. Fluorescence microscopes are useful for tracking the location of small molecules in samples with different binding sites. The microscope has two pinhole apertures at confocal positions, providing higher resolution compared to other optical microscopes. The second pinhole, in the focal plane, selects only the light from the focal point, which is collected by the objective. The advantage of the CLSM microscopes is their capacity of imaging the sample in a hydrated state.

1.6. Objective

The aim of this research is to study the effect of CB[7] as an additive on the properties of the NaDC hydrogel. In the previous studies, a more hydrophobic additive, CB[6], was used, with results indicating its predominance in the immobile, hydrophobic region of the gel.[39] Conversely, CB[7], being more hydrophilic, is hypothesized to reside in the mobile phase of the gel and serve as a carrier for small molecules from the hydrogel to the surrounding medium. The study will involve an analysis of different parts within the hydrogel, including its immobile gel network and dynamic aggregates. Structural analysis of the hydrogel will be conducted using CLSM. Kinetic investigations will focus on the dissociation rate constant of a guest molecule from CB[7] in the presence of NaDC aggregates using stopped-flow techniques in solutions. Furthermore, the binding behavior of guest molecules to CB[7] and the primary and secondary aggregates of NaDC will be analyzed using UV-VIS absorption and steady-state fluorescence spectroscopy. The ability of CB[7] to change the transport of small molecules from the hydrogel to the surrounding medium can significantly influence the release profiles of drugs, ultimately leading to more effective and controlled delivery systems.

1.7. References

(1) Bohne, C. Supramolecular Dynamics. *Chem. Soc. Rev.* **2014**, *43*, 4037-4050.
(2) Webber, M. J.; Langer, R. Drug Delivery by Supramolecular Design. *Chem. Soc. Rev.* **2017**, *46*, 6600-6620.
(3) Wu, J.; Peng, M.; Mu, M.; Li, J.; Yin, M. Perylene Diimide Supramolecular Aggregates: Constructions and Sensing Applications. *Supramol. Mater.* **2023**, *2*, 100031.
(4) Tang, H.; Thomas, S. S.; Wolf, L.; Natarajan, P.; Ko, Y. H.; Wilson, J.; Kim, K.; Bohne, C. Nonlinear Dependence on Na^+ Ions for the Binding Dynamics of Cucurbit[6]uril with the trans-1-Methyl-4-(4-hydroxystyryl)pyridinium Cation. *J. Phys. Chem. B* **2020**, *124*, 10219-10225.
(5) Philp, D.; Stoddart, J. F. Self-Assembly in Natural and Unnatural Systems. *Angew. Chem. Int. Ed.* **1996**, *35*, 1154-1196.
(6) Packwood, D. M.; Han, P.; Hitosugi, T. Chemical and Entropic Control on the Molecular Self-assembly Process. *Nat. Commun.* **2017**, *8*, 14463.
(7) Ernst, M.; Gryn'ova, G. Strength and Nature of Host-Guest Interactions in Metal-Organic Frameworks from a Quantum-Chemical Perspective. *ChemPhysChem* **2022**, *23*, e202200098.
(8) Zia, V.; Rajewski, R. A.; Stella, V. J. Effect of Cyclodextrin Charge on Complexation of Neutral and Charged Substrates: Comparison of (SBE)7M-β-CD to HP-β-CD. *Pharm. Res.* **2001**, *18*, 667-673.
(9) Steed, J. W. Supramolecular Gel Chemistry: Developments Over the Last Decade. *Chem. Commun.* **2011**, *47*, 1379-1383.
(10) Hussain, S.; Maktedar, S. S. Structural, Functional and Mechanical Performance of Advanced Graphene-Based Composite Hydrogels. *Results Chem.* **2023**, *6*, 101029.
(11) Chelu, M.; Musuc, A. M. Polymer Gels: Classification and Recent Developments in Biomedical Applications. *Gels* **2023**, *9*, 161.
(12) Thapliyal, P. C.; Singh, K. Aerogels as Promising Thermal Insulating Materials: An Overview. *J. Mater.* **2014**, *2014*, 127049.
(13) Lee, K. H.; Arshad, Z.; Dahshan, A.; Alshareef, M.; Alsulami, Q. A.; Bibi, A.; Lee, E.-J.; Nawaz, M.; Zubair, U.; Javid, A. Porous Aerogel Structures as Promising Materials for Photocatalysis, Thermal Insulation Textiles, and Technical Applications: A Review. *Catalysts* **2023**, *13*, 1286.
(14) Kuzina, M. A.; Kartsev, D. D.; Stratonovich, A. V.; Levkin, P. A. Organogels versus Hydrogels: Advantages, Challenges, and Applications. *Adv. Funct. Mater.* **2023**, *33*, 2301421.
(15) Aydınoğlu, D. Investigation of pH-Dependent Swelling Behavior and Kinetic Parameters of Novel Poly(acrylamide-co-acrylic acid) Hydrogels with Spirulina. *e-Polym.* **2015**, *15*, 81-93.
(16) Mohan, A.; Santhamoorthy, M.; Phan, T. T. V.; Kim, S.-C. pNIPAm-Based pH and Thermoresponsive Copolymer Hydrogel for Hydrophobic and Hydrophilic Drug Delivery. *Gels* **2024**, *10*, 184.
(17) Bustamante-Torres, M.; Romero-Fierro, D.; Arcentales-Vera, B.; Palomino, K.; Magaña, H.; Bucio, E. Hydrogels Classification According to the Physical or Chemical Interactions and as Stimuli-Sensitive Materials. *Gels* **2021**, *7*, 182.
(18) Corrente, F.; Paolicelli, P.; Matricardi, P.; Tita, B.; Vitali, F.; Casadei, M. A. Novel pH-Sensitive Physical Hydrogels of Carboxymethyl Scleroglucan. *J. Pharm. Sci.* **2012**, *101*, 256-267.
(19) Pita-López, M. L.; Fletes-Vargas, G.; Espinosa-Andrews, H.; Rodríguez-Rodríguez, R. Physically Cross-Linked Chitosan-Based Hydrogels for Tissue Engineering Applications: A State-of-the-Art Review. *Eur. Polym. J.* **2021**, *145*, 110176.

(20) Constantin, M.; Bucatariu, S.-M.; Doroftei, F.; Fundueanu, G. Smart Composite Materials Based on Chitosan Microspheres Embedded in Thermosensitive Hydrogel for Controlled Delivery of Drugs. *Carbohydr. Polym.* **2017**, *157*, 493-502.
(21) Malik, N. A. Solubilization and Interaction Studies of Bile Salts with Surfactants and Drugs: a Review. *Appl. Biochem. Biotechnol.* **2016**, *179*, 179-201.
(22) Small, D. M.; Penkett, S. A.; Chapman, D. Studies on Simple and Mixed Bile Salt Micelles by Nuclear Magnetic Resonance Spectroscopy. *Biochim. Biophys. Acta - Lipids Lipid Metab.* **1969**, *176*, 178-189.
(23) C. Ju, C. Bohne. Probing Bile Salt Aggregates by Fluorescence Quenching *Photochem. Photobiol.* **1996**, *63*, 60-67.
(24) Kalyanasundaram, K.; Thomas, J. K. Environmental Effects on Vibronic Band Intensities in Pyrene Monomer Fluorescence and Their Application in Studies of Micellar Systems. *J. Am. Chem. Soc.* **1977**, *99*, 2039-2044.
(25) Mazer, N. A.; Carey, M. C.; Kwasnick, R. F.; Benedek, G. B. Quasielastic Light Scattering Studies of Aqueous Biliary Lipid Systems. Size, Shape, and Thermodynamics of Bile Salt Micelles. *Biochemistry* **1979**, *18*, 3064-3075.
(26) Santos, C. S.; Miller, A. C.; Pace, T. C. S.; Morimitsu, K.; Bohne, C. Photochromism of a Spiropyran and a Diarylethene in Bile Salt Aggregates in Aqueous Solution. *Langmuir* **2014**, *30*, 11319-11328.
(27) Hofmann, A. F.; Mysels, K. J. Bile Salts as Biological Surfactants. *Colloids Surf.* **1987**, *30*, 145-173.
(28) Li, R.; Carpentier, E.; Newell, E. D.; Olague, L. M.; Heafey, E.; Yihwa, C.; Bohne, C. Effect of the Structure of Bile Salt Aggregates on the Binding of Aromatic Guests and the Accessibility of Anions. *Langmuir* **2009**, *25*, 13800-13808.
(29) Yihwa, C.; Bohne, C. Effect of Solvent Polarity and Viscosity on the Guest Binding Dynamics with Bile Salt Aggregates. *Photochem. Photobiol.* **2007**, *83*, 494-502.
(30) Yihwa, C.; Quina, F. H.; Bohne, C. Modulation with Acetonitrile of the Dynamics of Guest Binding to the Two Distinct Binding Sites of Cholate Aggregates. *Langmuir* **2004**, *20*, 9983-9991.
(31) Valenta, C.; Nowack, E.; Bernkop-Schnürch, A. Deoxycholate-hydrogels: Novel Drug Carrier Systems for Topical Use. *Int. J. Pharm.* **1999**, *185*, 103-111.
(32) McNeel, K. E.; Das, S.; Siraj, N.; Negulescu, I. I.; Warner, I. M. Sodium Deoxycholate Hydrogels: Effects of Modifications on Gelation, Drug Release, and Nanotemplating. *J. Phys. Chem. B.* **2015**, *119*, 8651-8659.
(33) Li, P.; Malveau, C.; Zhu, X. X.; Wuest, J. D. Using Nuclear Magnetic Resonance Spectroscopy to Probe Hydrogels Formed by Sodium Deoxycholate. *Langmuir* **2022**, *38*, 5111-5118.
(34) Jover, A.; Meijide, F.; Rodríguez Núñez, E.; Vázquez Tato, J. Aggregation Kinetics of Sodium Deoxycholate in Aqueous Solution. *Langmuir* **1998**, *14*, 4359-4363.
(35) Seyedalikhani, M. Exploring the Binding of Small Guest Molecules in Sodium Deoxycholate Hydrogels PhD University of Victoria, 2016. http://hdl.handle.net/1828/7615.
(36) Sun, X.; Xin, X.; Tang, N.; Guo, L.; Wang, L.; Xu, G. Manipulation of the Gel Behavior of Biological Surfactant Sodium Deoxycholate by Amino Acids. *J. Phys. Chem. B* **2014**, *118*, 824-832.
(37) Awasthi, A. A. A Photophysical Investigation on the Role of Complexity on Controlling the Functions of Pluronic F127 and Sodium Deoxycholate Supramolecular Hydrogels. PhD University of Victoria, 2023. http://hdl.handle.net/1828/15473.

(38) Masson, E.; Ling, X.; Joseph, R.; Kyeremeh-Mensah, L.; Lu, X. Cucurbituril Chemistry: A Tale of Supramolecular Success. *RSC Adv.* **2012**, *2*, 1213-1247.
(39) Talluri, S. G. Effect of Cucurbit[6]uril on the Structure and Dynamics of NaDC Gels. PhD University of Victoria, 2021. http://hdl.handle.net/1828/13847.
(40) Wang, X.; Zhang, S.; Zhao, H.; Wang, Q.; Zhang, Y.; Xu, H.; Xia, X.; Han, S. Spectroscopic Investigation into the Binding of Ferulic Acid with Sodium Deoxycholate: Hydrophobic Force Versus Hydrogen Bonding. *Langmuir* **2021**, *37*, 1420-1428.
(41) Pace, T. C. S.; Bohne, C. Dynamics of Guest Binding to Supramolecular Systems: Techniques and Selected Examples. *Adv. Phys. Org. Chem.* **2007**, *42*, 167-223.

Chapter 2: Effect of sodium deoxycholate on the dissociation process of berberine cation from cucurbit[7]uril

2.1. Introduction

2.1.1. Cucurbit[*n*]uril chemistry

Cucurbit[*n*]urils (CB[*n*]s) have attracted considerable interest among several macrocycles due to their wide range of uses in different fields, including biology, catalysis, and pharmacology.[1] CB[*n*]s have high binding affinities towards organic compounds compared to other macrocyclic hosts, such as β-cyclodextrin.[2] Among CB[*n*]s, CB[7] has a large cavity and high water solubility, which makes it a good host for small molecules.[1] Additionally, CB[7] is capable of binding to some guests very strongly through non-covalent interactions. For instance, adamantane guests can form complexes with CB[7] with equilibrium constants (K_{eq}) reaching up to 10^{17} M^{-1}. The 1-adamantylammonium (Ada^+) (Chart 2.1 (b)) complex with CB[7] has an association equilibrium constant of $(1.7 \pm 0.8) \times 10^{14}$ M^{-1} in water at a temperature of 298.15 K.[3]

a

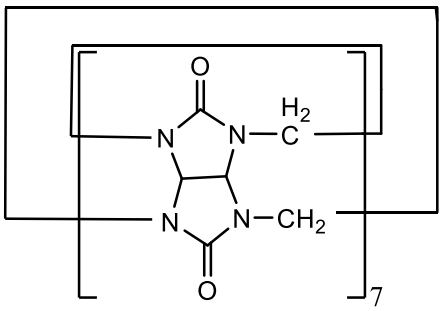

CB[7]

b

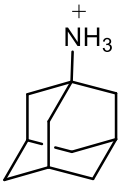

Ada^+

Chart 2.1. Molecular structures of (a) CB[7] and (b) Ada^+ cation.

While strong binding between guests and hosts is important, the equilibrium constant alone can only give information about the quantity of guests that can bind to the hosts at equilibrium. K_{eq} is defined as the ratio of the association rate constant (k_+) and the dissociation rate constant (k_-), and hence, the value of K_{eq} does not provide information about the dynamic processes of guest association and dissociation from the host (Equation 2.1). The K_{eq} value can

remain constant if both k_+ and k_- increase or decrease proportionally by the same amount; however, the kinetics of complex formation will be affected.[4] The knowledge on the kinetics is especially important when designing a delivery system in which the controlled dissociation of the guest from the delivery system is critical.[5]

$$K_{eq} = \frac{k_+}{k_-} \qquad \textbf{Equation 2.1}$$

2.1.2. Effect of metal ions on the binding kinetics of CB[*n*]s with guests

Previous studies in our group showed that adding metal ions changes the association and dissociation of organic molecules from CB[*n*]s. In these studies sodium cations were used in competition to the binding of guests to CB[7].[6, 7] The findings from these studies showed that the presence of other species, such as metal cations, has an impact on the kinetics of the binding of guest molecules to CB[7].

2.1.3. Sodium deoxycholate

Sodium deoxycholate (NaDC, Chart 2.2) which is the final product of the complicated chemical changes that occur during cholesterol metabolism,[8] can form a supramolecular hydrogel.[9] In aqueous solutions, NaDC molecules form supramolecular aggregates. The stability and structure of the NaDC aggregates are sensitive to temperature and pH.[10]

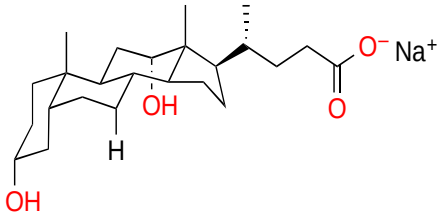

Chart 2.2. Molecular structure of NaDC.

At lower concentrations (4–6 mM) of NaDC, aggregates are formed that are called primary aggregates. Primary aggregate formation arises from the interaction involving the

hydrophobic face due to the presence of alkyl groups in the NaDC structure. As the concentration of NaDC molecules increases (8–12 mM), some of these primary aggregates further combine to form larger secondary aggregates.[11]

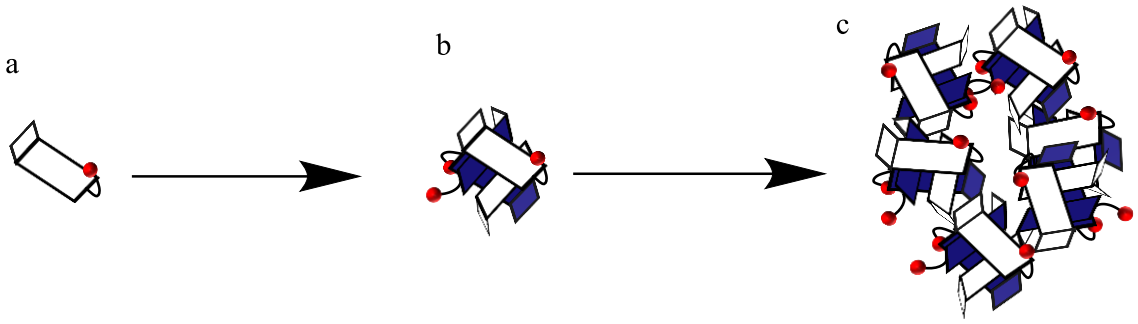

Scheme 2.1. Schematic representation of the formation of NaDC primary (b) and secondary (c) aggregates from NaDC monomers (a). Reprinted and modified with permission from Bohne's work.[14] Copyright (2009) American Chemical Society.

NaDC aggregates form different environments that can accommodate molecules with different properties within their structure by non-covalent interactions. NaDC aggregates have hydrophilic and hydrophobic binding sites within their structure. Primary aggregates are more hydrophobic. Secondary aggregates, on the other hand, are more hydrophilic.[13] Hence, both types of these aggregates can bind molecules differently based on the properties of the bound molecules. For example, hydrophobic molecules bind to the primary aggregates, while molecules containing hydrophilic moieties bind to the binding sites in secondary aggregates.[13] Binding of the small molecules to the bile salt aggregates depends on several factors, including the size, shape, and hydrophobic characteristics of the guests.[14]

The dissociation of guest molecules from a supramolecular system is complex, affected by various factors and identifying the primary parameters involved is essential for designing rational drug delivery systems. NaDC is a main component in the formation of a supramolecular hydrogel, which can be used as a drug delivery system. Understanding the interaction between small molecules and hydrogel building blocks, like NaDC hydrogel, is important for determining how these molecular-level interactions affect the release of small molecules from the hydrogel into the surrounding medium.

2.1.4. Fluorescent probes: binding, photophysical properties, and applications

A fluorescent probe is a type of molecule that binds to biological or chemical targets and shows a difference in its fluorescence properties when bound or unbound to the target. Depending on the structure and properties of the fluorophore, such as its excitation wavelength, pH,[15] and solvatochromic behavior[16] these molecules can be used to obtain useful information about the environment around the fluorophore. Fluorophores have been used in many fields of study, such as biology for cellular imaging,[17] chemical sensors,[18] and food science.[19] Moreover, fluorophores bind to different macrocycles, which changes the photophysical characteristics of the dye. These changes can be used to study the properties of the fluorophore-macrocycle complex, such as the determination of equilibriums constants or to establish the possible interactions occurring in the complex.[20]

2.1.4.1. Berberine as a fluorescence probe

Berberine (Chart 2.3), a natural isoquinoline alkaloid fluorophore with therapeutic applications, can bind to macrocycles.[21, 22] When berberine is unbound, it has a very low fluorescence quantum yield in water. However, the berberine's fluorescence intensity increases when it binds to specific macrocycles like CB[8], CB[7], and derivatives of calixarenes.[23, 24] Furthermore, changing the microenvironment around berberine to be more non-polar results to a shift in the steady-state fluorescence emission spectra towards shorter wavelengths.[22]

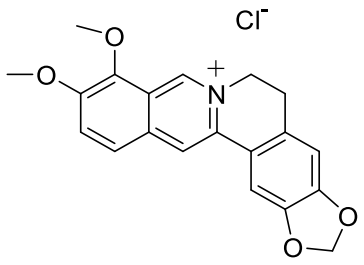

Chart 2.3. Molecular structure of berberine chloride.

2.1.5. Objective

The objective of this chapter is to investigate how the self-assembly of the NaDC aggregates affects the dynamics of berberine binding to CB[7]. NaDC aggregates are present in both the gel and aqueous phases of the hydrogel. Larger aggregates are immobilized inside the gel structure, while smaller aggregates are mobile in the aqueous phase.[25, 26] In this chapter the dynamics of berberine binding to CB[7] and NaDC will be investigated in solutions and not gels, since mobile NaDC aggregates are known to be present in NaDC gels. The experiments in solution were the starting point to study the dynamics of gel components, while studies on the immobile phase of the gel would be the subject of the following chapter.

Steady-state fluorescence and UV-VIS spectroscopy were used to identify the presence of different berberine species in an equilibrium state, including berberine binding to CB[7] and NaDC primary and secondary aggregates. Kinetic studies were done using the stopped-flow technique, in which the dynamics of berberine with NaDC and berberine complexed with CB[7] in the presence of NaDC aggregates were investigated.

2.2. Experimental Section

2.2.1. Materials

CB[7] (80%) was synthesized and purified by standard protocols in the Bohne group.[27] NaDC (Fluka, > 98%), sodium chloride (NaCl, Sigma-Aldrich, BioXtra, ≥ 99.5%), deionized water (Barnstead NANOpure deionizing systems, ≥ 17.8 MΩ cm^{-1}), 1-adamantylamine (Ada, Sigma-Aldrich, 97%), berberine chloride (Sigma-Aldrich, 98 %) and methanol (Fisher, spectral grade, ≥ 99.9%) were used as received.

2.2.2. Sample preparation

Stock solutions of NaDC (0.2 M) were prepared by dissolving 82.92 mg NaDC in 1 mL deionized water. Stock solutions of NaCl (0.2 M) were prepared by adding 58 mg NaCl to 5 mL deionized water. Stock solutions of Ada (1 mM) were prepared by adding 0.75 mg Ada to 5 mL deionized water which results in the protonation of this compound (adamantylammonium cation, Ada^+, $pK_a \approx 10.3$). Stock solutions of CB[7] (0.2 mM) were made by adding 2.9 mg CB[7] to 10 mL deionized water. Stock solutions of berberine (0.5 mM) were made by adding 0.925 mg berberine chloride to 5 mL spectroscopic grade methanol. All samples used in the experiments were prepared using the methods described below one day before the experiments and the temperature for all experiments was kept at 20 °C.

For stopped-flow experiments, solutions were prepared in volumetric flasks, and the final concentrations were obtained by mixing the solutions from two syringes at a 1:1 ratio. Appropriate amounts of stock solutions of berberine chloride, CB[7], NaDC and NaCl were added to the volumetric flask, and the volumes were completed to 10 or 25 mL using deionized water. Final concentrations of CB[7] and berberine were 0.75 and 0.25 μM, respectively. The final concentrations of Ada^+ were 2, 5, 10, 20, 40, and 80 μM. Final concentrations of NaDC were between 1 and 25 mM. The total concentration of Na^+ in all samples, arising from NaDC and NaCl, was kept constant at 50 mM.

Solutions for steady-state fluorescence and absorption experiments were made in 3-dram sample vials. Appropriate amounts of stock solutions of berberine chloride, CB[7], NaDC and NaCl were added to the sample vials, and the volume was completed to 3 mL. Final concentrations of berberine were 0.25 and 10 μM. The final concentrations of CB[7] were 0.25,

1, 5, 10, 30 μM. Final concentrations of NaDC were between 1 and 50 mM. The final concentrations of Ada^{+} were 40 and 80 μM.

2.2.3. Instrumentation

Emission spectra were collected on a PTI QM-40 spectrophotometer using 10 × 10 mm quartz cells. The excitation wavelengths for the collection of the emission spectra were 280, 345, 400, and 420 nm with the collection of the emission ranging between 400 to 750 nm. The excitation spectra were measured using the emission wavelengths of 490, 500, and 650 nm with the detection ranging between 250 to 650 nm. The step size was 0.5 nm, the integration time was set to 0.25 s. The excitation and emission monochromator bandwidths were set to 2 and 5 nm.

Kinetic studies were conducted on an Applied Photophysics SX20 stopped-flow system using a Hg-Xe vapour lamp as the excitation source. The samples were irradiated at 345 nm and the monochromator bandwidth was set to 4.65 nm. Fluorescence emission was detected using a cutoff optical filter that selectively transmits light with wavelengths longer than 395 nm. The high voltage was adjusted to achieve a maximum signal of around 5 V. For each kinetic trace, 16 individual traces were averaged.

2.2.4. Data analysis for stopped-flow experiments

In a stopped-flow experiment, two or more reactants are rapidly mixed. This mixing initiates the reaction, and the progress of the reaction is monitored over time. The resulting kinetic trace shows how the concentrations of species in the mixed solution change over time. The observables used to monitor the change in concentrations are fluorescence intensity values. The averaged kinetic traces were fit to the sum of exponential function equation (Equation 2.2).

$$\Delta I = a_0 + a_1 e^{-k_{obs1}t} + a_2 e^{-k_{obs2}t} + a_3 e^{-k_{obs3}t} \qquad \textbf{Equation 2.2}$$

Where, *k* values are observed rate constant for each kinetic component labelled with a number, *a* values correspond to the amplitudes of each component, and a_0 is the offset. This equation is a general one, but my data fit single exponential kinetics. All traces obtained were fitted to a monoexponential function, leading to the recovery of one observed rate constant and one amplitude.

2.2.5. Checking for the purity of berberine

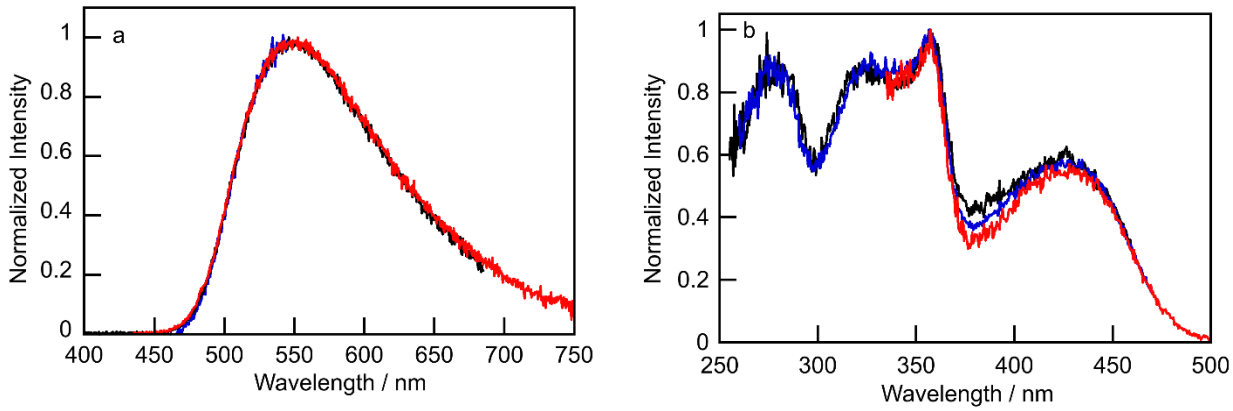

Figure 2.1. (a) Normalized steady-state fluorescence emission spectra of 30 μM berberine (λ_{ex} = 280 nm (black), 345 nm (blue), 400 nm (red)) in methanol. (b) Normalized steady-state fluorescence excitation spectra of 30 μM berberine in methanol normalized at 450 nm collected at different emission wavelengths (λ_{em} = 490 nm (black), 500 nm (blue), 650 nm (red)).

The purity of berberine was checked in fluorescence experiments to establish that fluorescent impurity was not present, which would interfere with the experiments. By varying the excitation or emission wavelengths, it becomes possible to identify additional peaks or spectral changes that do not correspond to the spectra of the pure molecule. These variations in excitation or emission spectra can result from contaminants that show fluorescence. The emission spectra did not change when the sample was excited at different wavelengths (Figure 2.1 (a)). Excitation spectra of berberine at different emission wavelengths show a negligible change around 360 nm (Figure 2.1 (b)) when the samples were detected at different emission wavelength.

2.3. Results

2.3.1. Absorption and steady-state fluorescence measurements

2.3.1.1. Effect of the addition of NaDC on the berberine steady-state fluorescence and absorption spectra

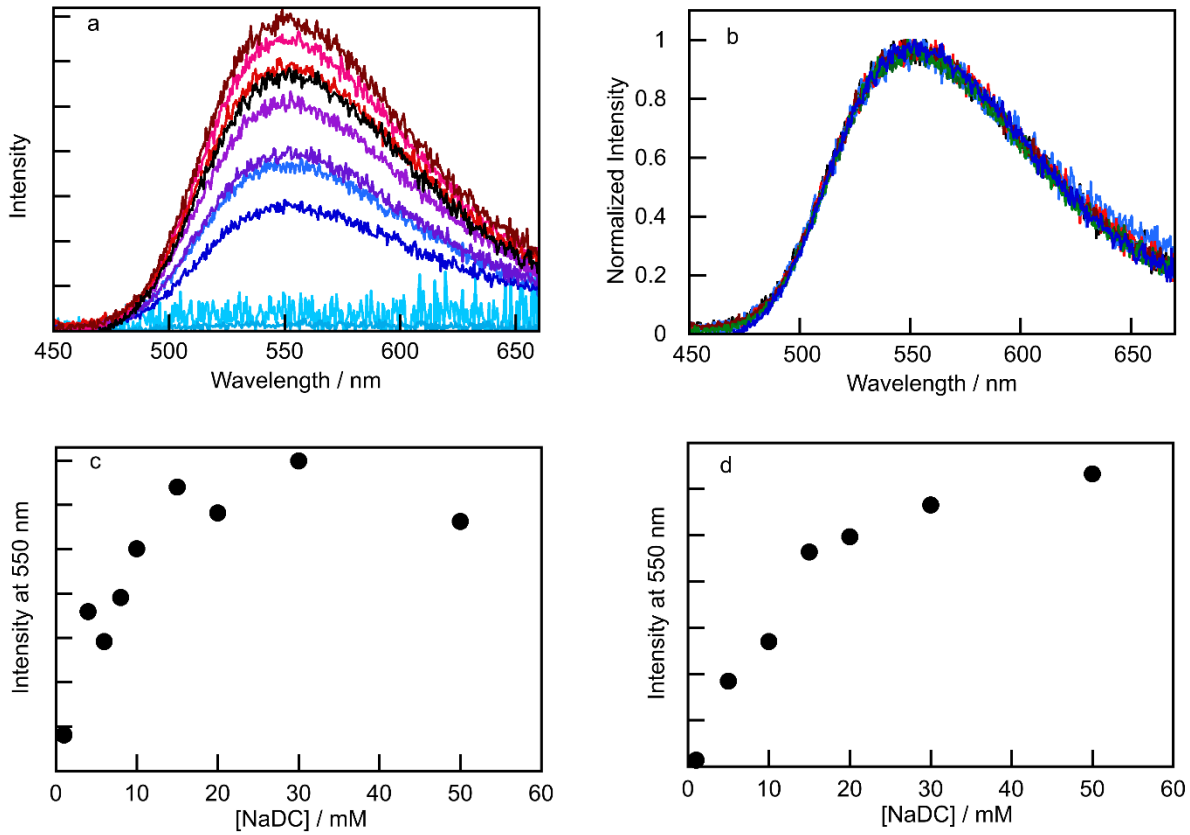

Figure 2.2. (a) Steady-state fluorescence emission spectra of 0.25 μM berberine (λ_{ex} = 345 nm) with (0, 1, 4, 6, 8, 10 mM) NaDC shown as a blue gradient (from light blue to violet) and (15, 20, 30, 50 mM) NaDC in red gradient (from pink to black). (b) Normalized steady-state fluorescence emission spectra of 0.25 μM berberine (λ_{ex} = 345 nm) with increasing NaDC concentrations shown in panel (a). (c, d) Fluorescence emission intensity at 550 nm for different concentrations of NaDC for two independent experiments. The plot shown in panel (c) is derived from data in panel (a) and panel (d) is derived from the data shown in the appendix (Figure A2.1).

The addition of NaDC at concentrations in which the monomer, primary, and secondary aggregates are present led to changes of the steady-state fluorescence emission intensity of berberine (Figure 2.2 (a)). However, the shape of the emission spectra of berberine did not change as the NaDC concentration was raised (Figure 2.2 (b)). The increase in the berberine emission intensity slowed down in high NaDC concentrations (Figures 2.2 (c) and (d), [NaDC] = 30 mM). No quantitative analysis is possible because of the scatter in the data caused by the difficulties in subtracting the spectra for the control experiments.

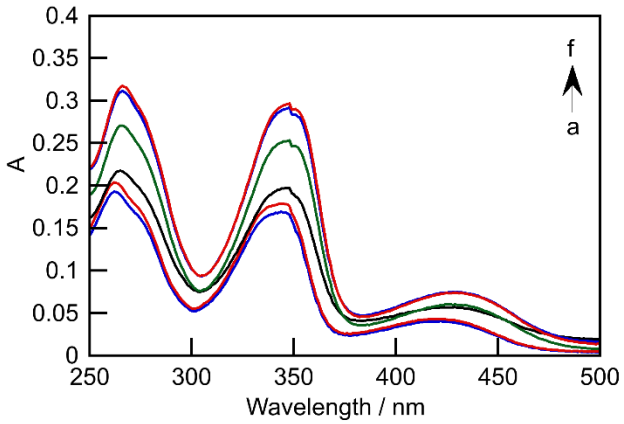

Figure 2.3. Absorption spectra of 10 μM berberine in the absence (a, blue) and presence of 1, 4, 8, 20, 50 mM (b–f) NaDC ([Na^+] = 50 mM).

The absorption spectra of berberine shows three distinct peaks around 263 nm, 343 nm, and 421 nm.[28] Upon the addition of NaDC, a bathochromic shift for the peaks at 343 and 421 nm was observed in the absorption spectra of berberine (Figure 2.3). The shift in the absorbance maxima after the addition of NaDC indicates the binding between berberine and NaDC primary and secondary aggregates. This shift to longer absorption wavelength indicates a change in the polarity of berberine's microenvironment to a less polar environment than in water.[22, 29]

2.3.1.2. Optimization of the excitation wavelength for berberine after binding to CB[7] and NaDC

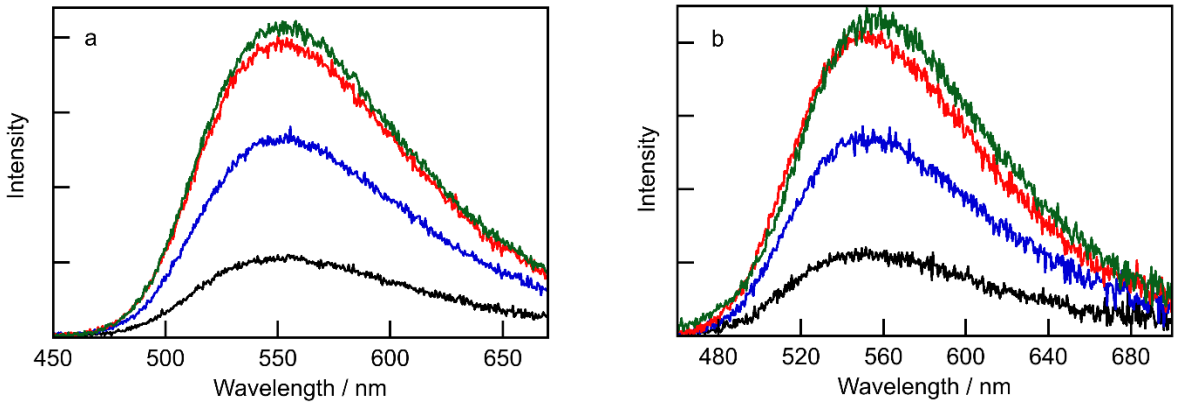

Figure 2.4. Steady-state fluorescence emission spectra of 0.25 μM berberine with an excitation wavelength of (a) 345 nm and (b) 420 nm with 5 (black), 10 (blue), 15 (red), 25 mM (green) NaDC ([Na^+] = 50 mM).

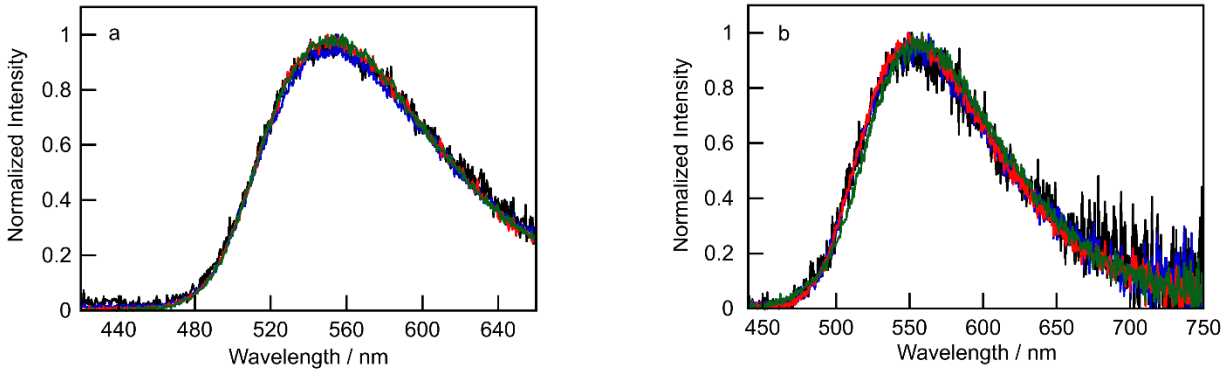

Figure 2.5. (a) Normalized steady-state fluorescence emission spectra of 0.25 μM berberine with an excitation wavelength of (a) 345 nm and (b) 420 nm, with 5 (black), 10 (blue),15 (red), 25 mM (green) NaDC ([Na^+] = 50 mM).

Previous studies investigating the photophysical properties of berberine used excitation wavelengths approximately at 345 nm and 420 nm.[30, 31] The effect of the excitation wavelength

on the emission spectra of berberine in the presence of NaDC was investigated and no changes in the shape of the emission spectra were observed for the samples excited at each of the wavelengths (Figure 2.4 and 2.5). The fact that the emission spectra of berberine do not change when excited at 345 nm or 420 nm, with different NaDC concentrations, shows that the microenvironment's polarity around berberine remains the same in NaDC solutions with varying primary and secondary aggregate concentrations. If berberine molecules were distributed in microenvironments with different polarities, a change would have been observed for the emission spectra when berberine was excited with different wavelengths.

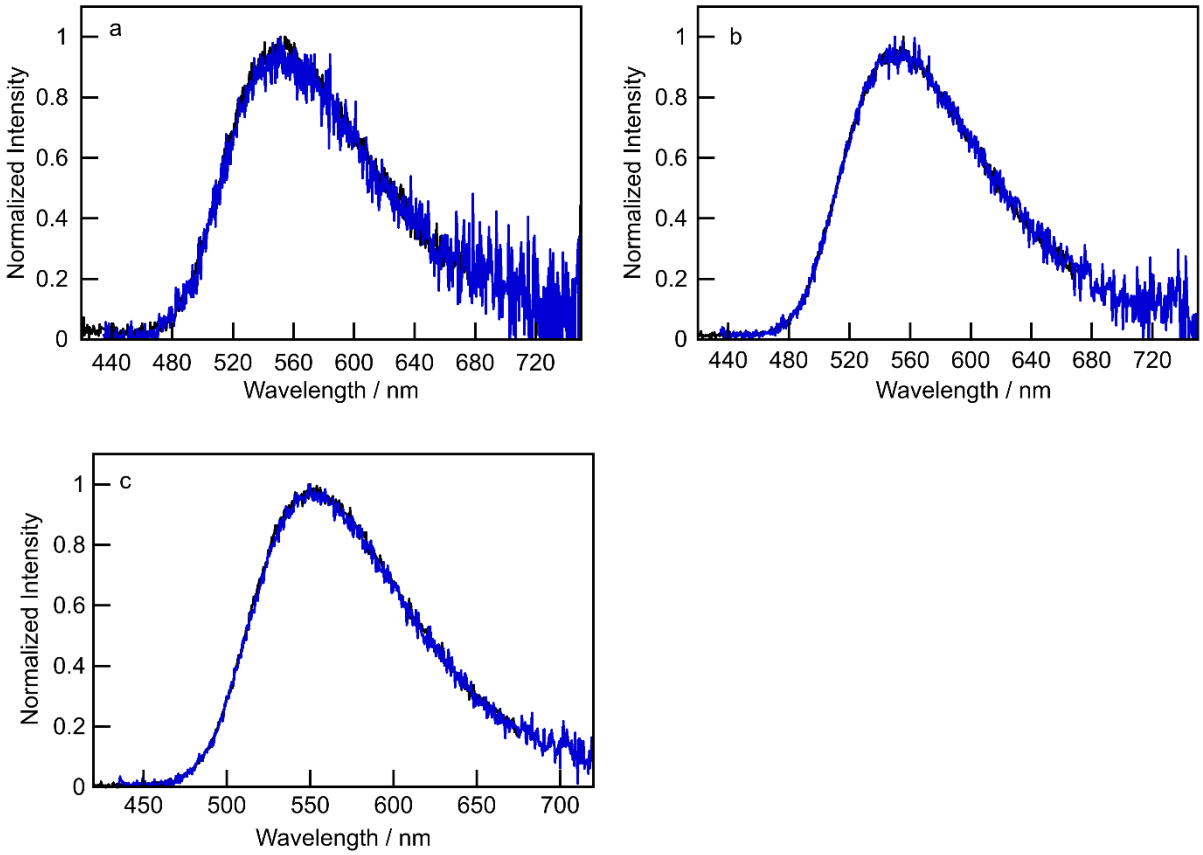

Figure 2.6. Normalized steady-state fluorescence emission spectra of 0.25 μM berberine (λ_{ex} = 345 nm, black; 420 nm, blue) with 5 (a), 10 (b), 15 mM (c) NaDC ([Na^+] = 50 mM).

There is no shift in the normalized emission spectra of berberine with different concentrations of NaDC that were excited with two different wavelengths (Figure 2.6). Changing the NaDC concentration from 5 mM, where only primary aggregates are present, to 10 and 15

mM, where secondary aggregates are also present, did not lead to a change in the normalized emission spectra of berberine.

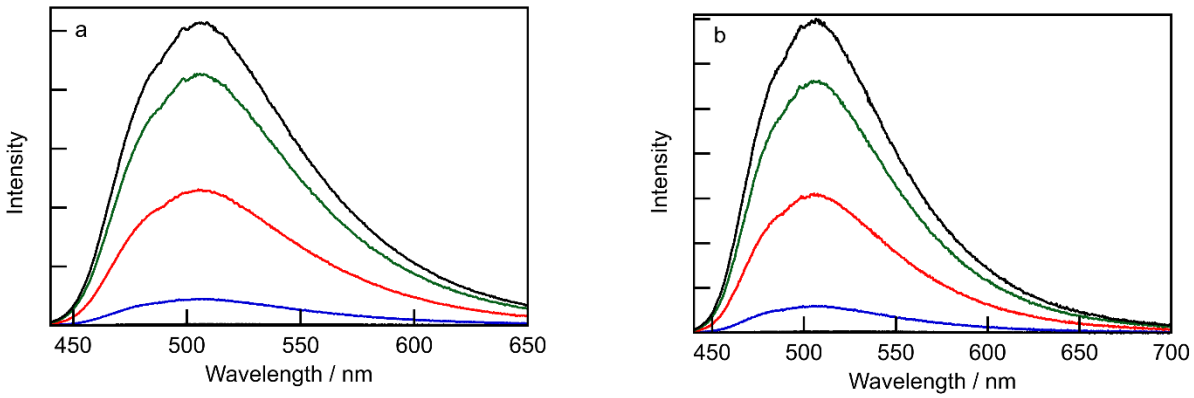

Figure 2.7. Steady-state fluorescence emission spectra of 10 μM berberine with an excitation wavelength of (a) 345 nm and (b) 420 nm with 1 (blue), 5 (red), 10 (green), 30 μM (black) CB[7].

Berberine forms a 1:1 inclusion complex with CB[7], and this binding leads to a 500-fold enhancement in the berberine's steady-state fluorescence emission intensity.[24] The increase in fluorescence intensity when berberine forms complexes with CB[7] is due to the rigid structure of the berberine's surroundings inside the CB[7] cavity. This rigidity reduces pathways for nonradiative decay, leading to an enhanced fluorescence intensity. There is no shift in the steady-state fluorescence emission spectra upon binding of berberine with CB[7], when berberine is excited at 345 and 420 nm (Figure 2.7). This finding shows that berberine in the presence of CB[7] has a consistent structural conformation and binding behavior regardless of the excitation wavelength used.

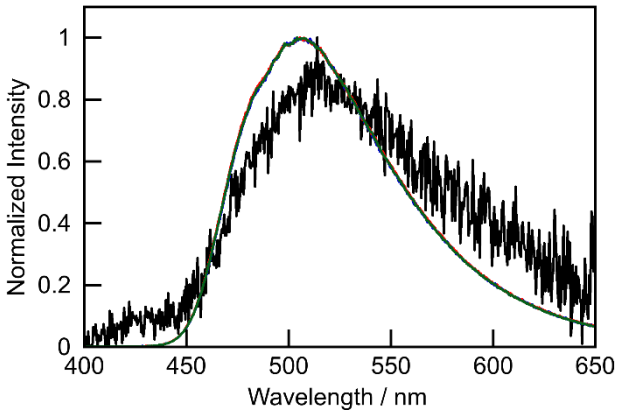

Figure 2.8. Normalized steady-state fluorescence emission spectra of 10 μM berberine (λ_{ex} = 345 nm) with 0 (black), 5 (blue), 20 (red), 30 μM (green) CB[7]. Spectra for 5, 20, 30 μM CB[7] are overlapping. The low signal to noise ratio in the spectrum of berberine with 0 μM CB[7] is attributed to the low emission quantum yield of free berberine in water.

Normalized emission spectra of berberine, with and without CB[7], show that berberine emission undergoes a hypochromic shift from around 510 to 500 nm upon binding to CB[7] (Figure 2.8). The hypochromic shift of berberine emission is characteristic of berberine when present in a less polar environment compared to water.[22] In addition, there is no shift in the maximum emission wavelength with different concentrations of CB[7], showing that even at higher concentrations of CB[7], the same complex is formed between berberine and CB[7] as observed at lower concentrations of the CB[7].

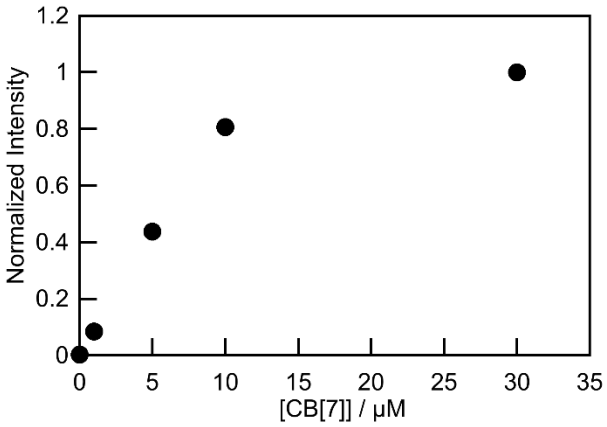

Figure 2.9. Plot for the dependence of the steady-state fluorescence 10 μM berberine (λ_{ex} = 345 nm) bound to different concentrations of CB[7], normalized to the emission at 500 nm of the highest concentration of CB[7].

Addition of CB[7] to a solution containing berberine led to an increase in the emission intensity of berberine when the CB[7] concentration was raised (Figure 2.9). The intensity increase leveled off at higher CB[7] concentrations as expected for the formation of a 1:1 berberine-CB[7] complex.[24] Complete binding of berberine was achieved when the concentration of CB[7] was three times higher than that of berberine.

2.3.1.3. Effect of CB[7] on the absorption spectrum of berberine

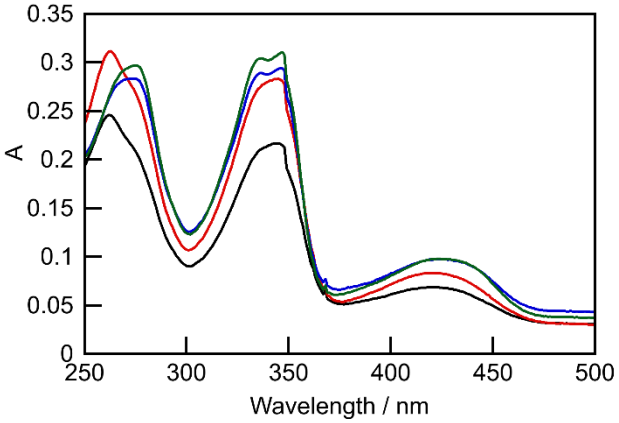

Figure 2.10. Absorption spectra of 10 μM berberine with 0 (black), 1 (red), 10 (blue), 30 μM (green) CB[7] ([Na+] = 50 mM).

The absorption spectra of berberine with increasing CB[7] concentrations show that the absorption maxima of berberine changes upon addition of CB[7] (Figure 2.10). This change in the absorption spectra of berberine shows that there is an interaction in the ground state between berberine and CB[7].

2.3.1.4. Relocation of berberine with the addition of NaDC from the berberine@CB[7] complex

The addition of NaDC to a solution containing the berberine@CB[7] complex leads to a change in the steady-state fluorescence emission spectra (Figure 2.11). By increasing the NaDC concentration, the emission maxima shift from around 510 nm to 550 nm (Figure 2.11 (a, c)), along with a decrease in the maximum emission intensity (Figure 2.11 (a)). At the highest NaDC concentration tested, a small band appears at 510 nm, indicating that some berberine remains bound to CB[7], while most has moved to NaDC aggregates.

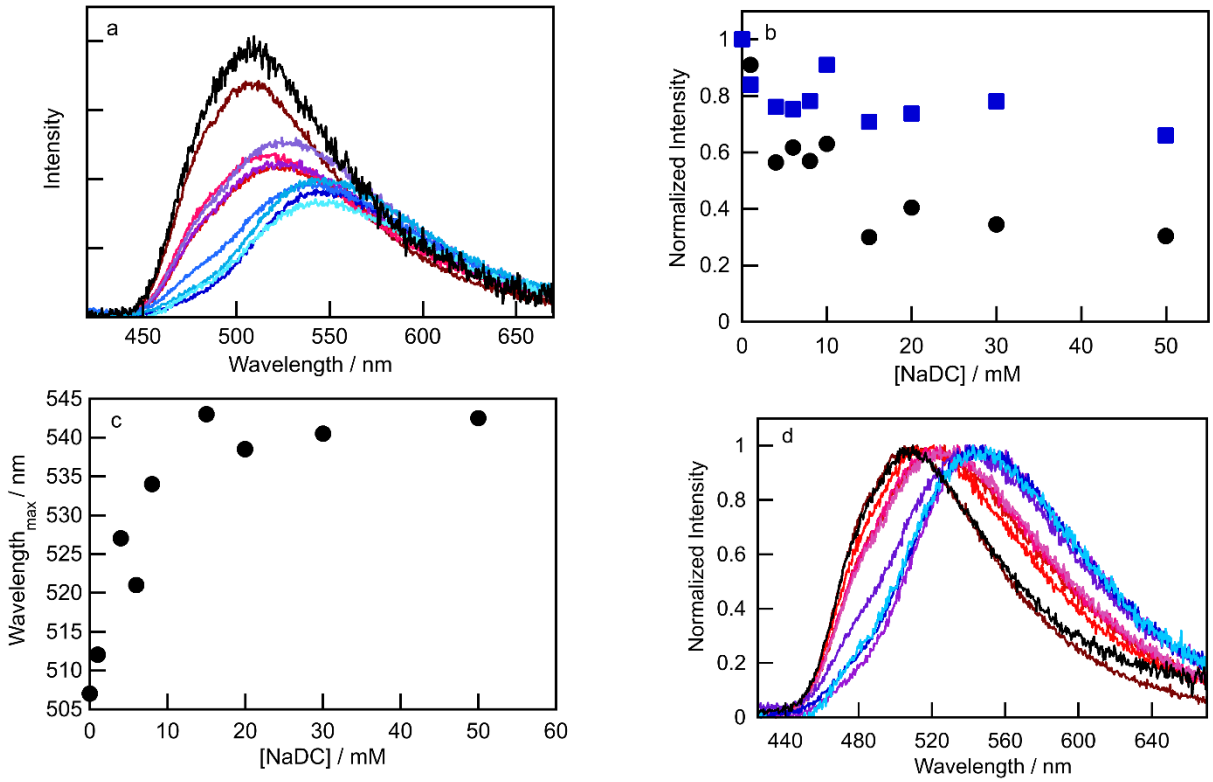

Figure 2.11. (a) Steady-state fluorescence emission spectra of 0.25 μM berberine (λex = 345 nm) and 0.75 μM CB[7] in the absence (black) and presence of low concentrations (1, 4, 6 mM) of NaDC shown as a red gradient from dark red to pink, and higher concentrations (8, 10, 15, 30, 50 mM) of NaDC shown as a blue gradient from purple to light blue. (b) Fluorescence intensities of the 0.25 μM berberine (λex = 345 nm) and 0.75 μM CB[7] solution with different NaDC concentrations at 510 nm (black circle) and 550 nm (blue square). The intensities were normalized to the intensity of berberine@CB[7]. (c) Dependence of the maximum emission wavelength of berberine@CB[7] on the NaDC concentrations. (d) Normalized spectra for the emission of berberine@CB[7] at different NaDC concentrations. The data for panels (b),(c) and (d) were derived from the data in panel (a).

Free berberine and berberine bound to NaDC emit at around 550 nm (Figures 2.6), while the berberine complexed to CB[7] emits around 510 nm (Figures 2.8) The emission intensity at both of these wavelengths and also the emission maxima change with varying NaDC concentrations (Figure 2.11 (b,c)) for solutions containing berberine and CB[7]. Normalized emission spectra of berberine also show that the addition of NaDC to the berberine@CB[7] complex causes a shift in the maximum emission wavelength of berberine (Figure 2.11 (d)).

2.3.1.5. Effect of addition of Ada^+ on the berberine fluorescence when berberine is bound to NaDC

Ada^+ is a cationic and non-fluorescent guest known for its strong binding to CB[7].[3] The strong binding ability between CB[7] and Ada^+ plays an important role in displacing other guests complexed with CB[7]. Guests that show an increase in their fluorescence on binding to CB[7], like berberine, on displacement by Ada^+, will show a decrease in their emission intensity due to a change of berberine's quantum yield inside and outside of the CB[7] cavity.

In the microheterogeneous system containing CB[7] and NaDC aggregates, berberine is bound to both CB[7] and NaDC (Figure 2.11 (a)). However, there was no prior information regarding whether Ada^+ can displace berberine that is bound to NaDC aggregates. This information is required for the analysis of the kinetic data.

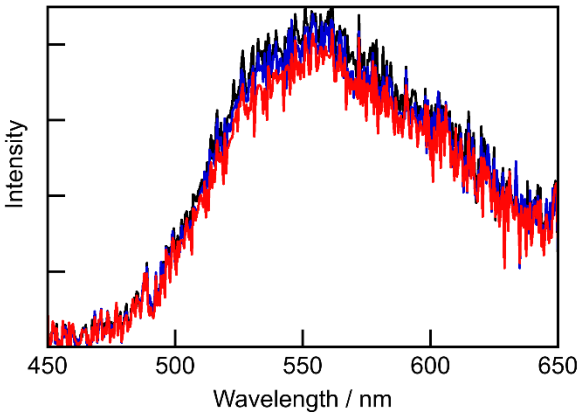

Figure 2.12. Steady-state fluorescence emission spectra of 0.25 μM berberine (λ_{ex} = 345 nm) with 25 mM NaDC with 0 (black), 40 (blue), 80 μM (red) Ada^+ ([Na^+] = 50 mM).

The emission spectra of berberine bound to NaDC were not affected when Ada^+ was added up to a concentration of 40 μM, indicating that Ada^+ did not displace berberine bound to NaDC aggregates (Figure 2.12). However, when the concentration of Ada^+ increased to 80 μM, a slight decrease in the emission intensity of berberine bound to NaDC was observed (red trace in Figure 2.12). This slight decrease in the emission intensity of berberine bound to NaDC, as the concentration of Ada^+ increased to 80 μM, suggests that at this high Ada^+ concentration, some berberine may be displaced from the NaDC aggregates.

2.3.2. Kinetic measurements

2.3.2.1. Analysis of the displacement kinetics of berberine from the complex with CB[7]

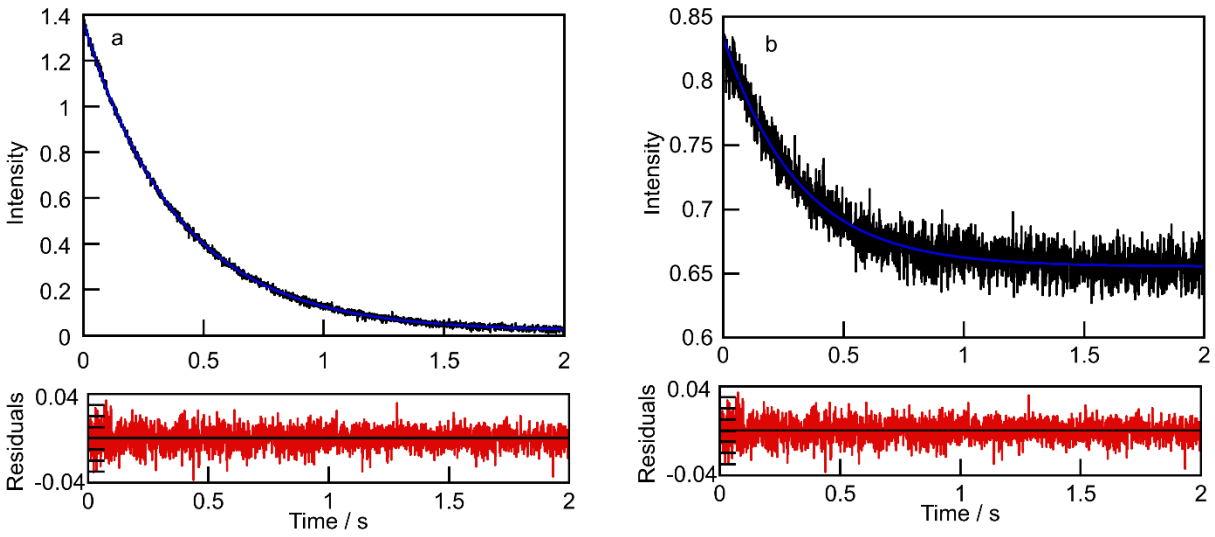

Figure 2.13. Kinetic traces (black) for the mixing of a solution containing 5 µM Ada+ with a solution containing of 0.25 µM berberine, 0.75 µM CB[7] and (a) 0 , (b) 25 mM NaDC ([Na+] = 50 mM). The fit of the experimental data to a monoexponential function is shown in blue and the residual between the experimental data and the fits are shown in the lower panels. All the concentrations mentioned are after mixing.

The analysis of kinetic traces involves fitting the data to a mathematical model (blue lines in Figure 2.13) from which rate constants are obtained. Residuals between the kinetic trace and the values obtained from the fit are calculated. If the mathematical model adequately fits the experimental data, then the residuals are random around zero. For the stopped-flow experiments described in this chapter, the traces show a random residual and fit to a mono-exponential decay model.

2.3.2.2. Determination of the association of berberine with NaDC aggregates

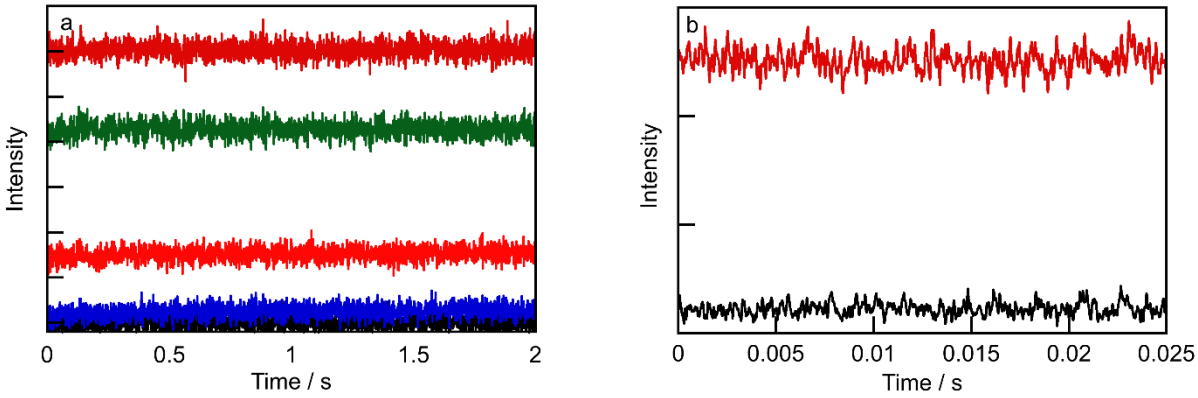

Figure 2.14. (a) Stopped-flow kinetic traces for the mixing of 0.25 μM berberine to 0 (black), 2 (blue), 15 (green), 25 mM (upper red) NaDC over a time scale of 2 s. (b) Stopped-flow kinetic traces for the mixing of 0.25 μM berberine in the absence (black) and presence (red) of 25 mM NaDC over a time scale of 0.025 s ([Na^+]= 50 mM).

Stopped-flow experiments were conducted to study the kinetics of association of berberine to NaDC aggregates. The association of berberine to NaDC aggregates cannot be observed due to the rapid kinetics of berberine binding, which occurs faster than the millisecond detection limit of the equipment (Figure 2.14). When the kinetics for a reaction is faster than the detection limit of the experiment, the instrument will not be able to capture the change of concentration over time. The change in concentration appears as a jump in the intensity followed by a flat line (Figure 2.14 (a, b)). The initial fluorescence intensity increased as the NaDC concentration was raised (Figure 2.14 (a)). The rise in initial intensity shows that berberine binds to NaDC aggregates within the 1 ms mixing time of the equipment.

2.3.2.3. Effect of Ada^+ addition on the berberine dissociation from the berberine@CB[7] complex in the presence of NaDC

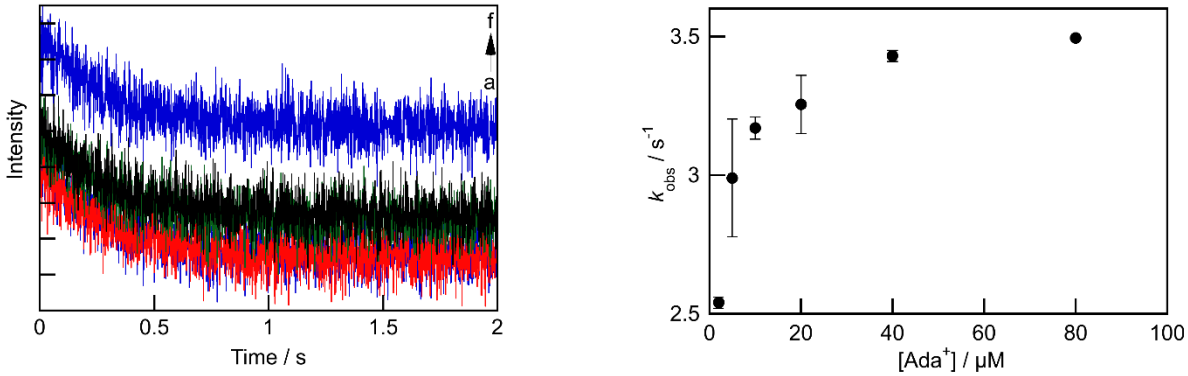

Figure 2.15. (a) Stopped-flow kinetic traces for the mixing of the solution containing 0.25 μM berberine, 0.75 μM CB[7] and 25 mM NaDC with 2 (a, lower black), 5 (b, lower blue), 10 (c, red), 20 (d, green), 40 (e, upper black), 80 μM (f, upper blue) Ada+ ([Na+] = 50 mM). All the concentrations mentioned are after mixing. Some of the traces are overlayed. (b) Averaged kobs values for two independent experiments obtained by fitting the data using a monoexponential decay function. The kobs values correspond the apparent dissociation rate constant (k_{-app}) values. The values shown are averages for the values obtained from the data in panel (a) and from Figure A2.2 in the appendix.

The effect of addition of NaDC to the kinetics of the displacement of berberine from the CB[7] complex were measured for different concentrations of Ada^+ (Figure 2.15 (a)). The k_{obs} values obtained from kinetic traces show that until the Ada^+ concentration reaches 40 μM, raising the Ada^+ concentration changes the k_{obs} that corresponds to the berberine dissociation from CB[7] in the presence of NaDC aggregates. The k_{obs} does not change significantly for Ada^+ concentrations of 40 μM or 80 μM (Figure 2.15 (b)).

2.3.2.4. Effect of the addition of NaDC on the displacement kinetics of berberine by Ada^+ from the berberine@CB[7] complex

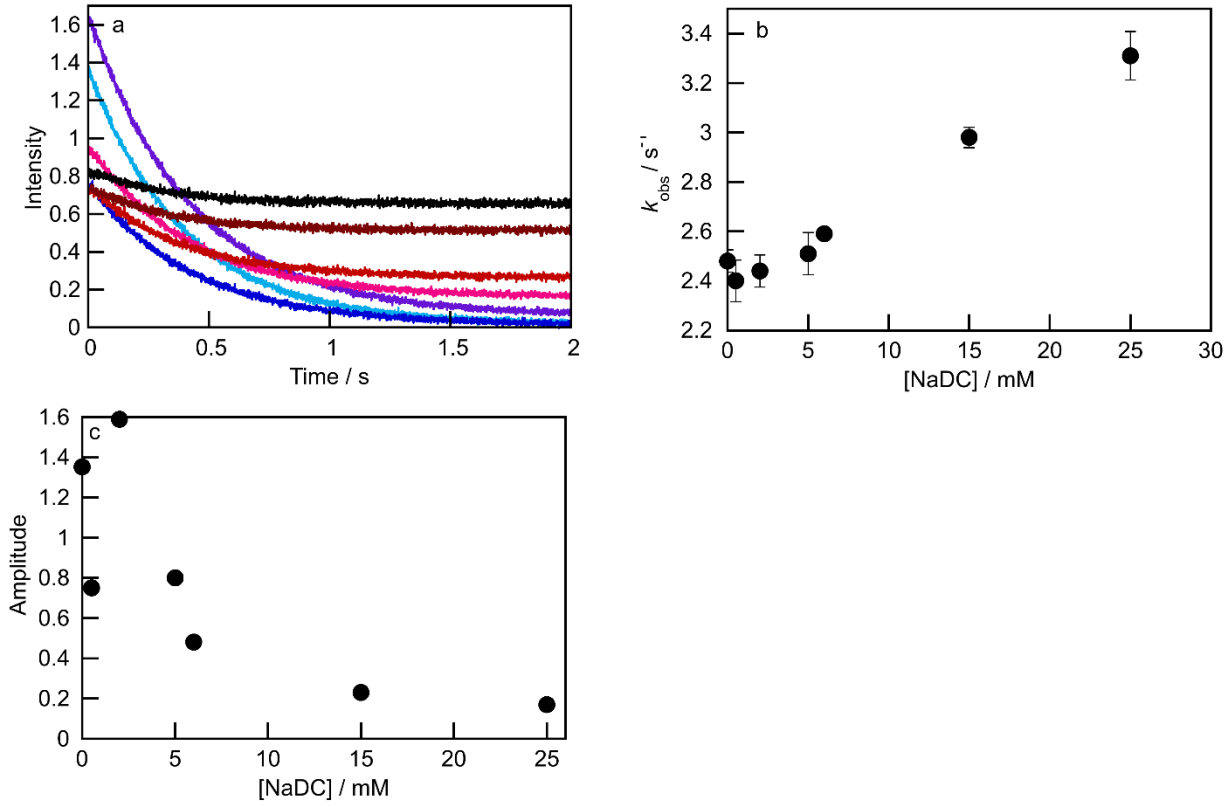

Figure 2.16. (a) Stopped-flow kinetic traces for the mixing of 5 μM Ada^+ with solutions containing 0.25 μM berberine, 0.75 μM CB[7] and different concentrations of NaDC. Lower concentrations of NaDC (0, 0.5, 2 mM) are shown as a blue gradient from light blue to purple and higher concentrations (5, 6, 15, 25 mM) are shown as a red gradient from pink to black ($[Na^+]$ = 50 mM). All concentrations mentioned are after mixing. (b) Averaged k_{obs} values from independent experiments obtained by fitting the data (panel (a) and appendix A 2.3) using a monoexponential decay function. Error bars that are not visible are smaller than the data point shown. (c) Amplitudes for traces in panel (a).

The kinetic traces of the dissociation of berberine from CB[7] by 5 μM Ada^+ change in the presence of different NaDC concentrations (Figure 2.16 (a)). By fitting the traces, the dissociation rate constant of berberine from CB[7] was found to be affected by the concentration of NaDC (Figure 2.16 (b)).

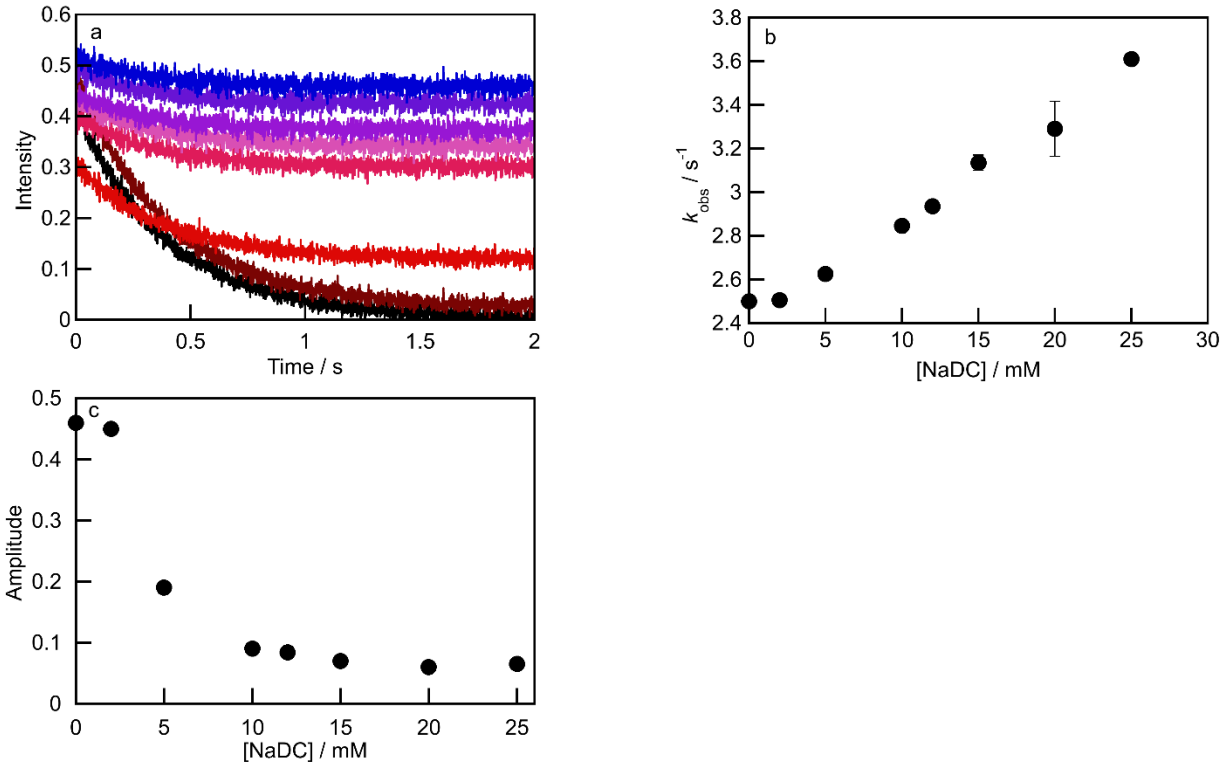

Figure 2.17. (a) Stopped-flow kinetic traces for the mixing of 40 μM Ada$^+$ with the solutions containing 0.25 μM berberine, 0.75 μM CB[7] and different concentrations of NaDC. Low concentrations of NaDC (0, 2, 5, 10, 12 mM) are shown as a red gradient from black to light pink and higher concentrations (15, 20, 25 mM) are shown as a blue gradient from light purple to blue ([Na$^+$] = 50 mM). All concentrations mentioned are for after mixing. (b) Averaged k_{obs} values from two independent experiments panel (a) and Figure A 2.4 obtained by fitting the data using a monoexponential decay function. Errors bars that are not visible are smaller than the data point shown. (c) Amplitudes for traces in panel (a).

The same kinetic experiments were conducted using a higher concentration of Ada$^+$ (Figure 2.17 (a)). In contrast to the experiments at the lower Ada$^+$ concentration, k_{obs} values increased continuously (Figure 2.17 (b)) and the amplitude of the kinetics decreased continuously (Figure 2.17 (c)). In addition, errors in the averaged k_{obs} values were smaller when the higher Ada$^+$ concentration was used.

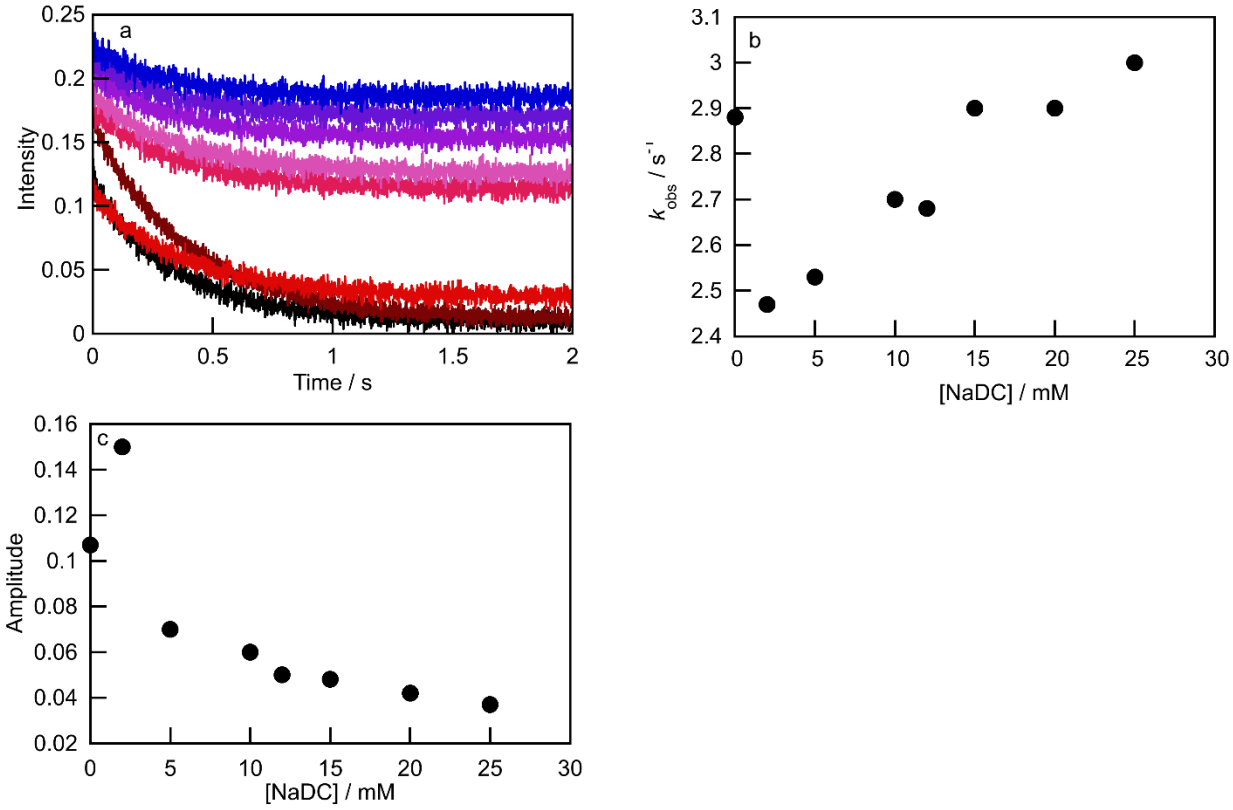

Figure 2.18. (a) Stopped-flow traces for the mixing of 80 µM Ada+ with the solutions containing 0.25 μM berberine, 0.75 µM CB[7] and different concentrations of NaDC. Lower concentrations of NaDC (0, 2, 5, 10, 12 mM) are in red gradient from black to light pink and higher concentrations (15, 20, 25 mM) are in blue gradient from light purple to blue ([Na+] = 50 mM). All the concentrations mentioned are for after mixing. (b) kobs obtained by fitting the data using a monoexponential decay function derived from data in panel (a). (c) Amplitudes for the traces in panel (a). Error bars are smaller than the data points shown.

Increasing the concentration of Ada^+ further to 80 μM led to different trends for the k_{obs} values and the amplitude of the kinetics (Figure 2.18). The values for k_{obs} initially decreased, followed by a discontinuous trend of increasing rate constants (Figure 2.18 (b)). Also, the trend for the amplitudes is not continuous (Figure 2.18 (c)).

2.4. Discussion

Studying the interactions between small molecules and the main building blocks of a supramolecular hydrogel is not the primary focus in fields like drug delivery system development. However, understanding how these molecules interact and how each component affects the dynamics and interactions of the small molecules to be released is important. This knowledge enhances our understanding of the function of supramolecular systems and ultimately help in the rational design of more effective delivery systems.

Steady-state fluorescence experiments of berberine with CB[7] (Figure 2.7) and berberine with NaDC aggregates (Figure 2.2) show that berberine binds to both of the CB[7] and NaDC aggregates. The maximum emission of berberine bound to CB[7] and NaDC aggregates differs due to the sensitivity of berberine's emission to the polarity of its microenvironment. When berberine enters the CB[7] cavity and forms a complex, the maximum emission of berberine changes to a shorter wavelength. When NaDC is added to the solution containing berberine and CB[7], the maximum emission shifts to a longer wavelength, indicating that some of the berberine has exited the non-polar cavity of CB[7] and is bound to the NaDC aggregates (Figure 2.11 (a)). Qualitative analysis of the wavelength shift of the berberine's steady-state fluorescence emission spectra in different microenvironments supports that berberine is distributed between the NaDC aggregates and CB[7] (Figure 2.11 (d)). In this microheterogeneous system, there are two hosts for berberine: CB[7], which acts as a rigid host, and NaDC aggregates, serving as a non-rigid host. A rigid host is one whose structure remains relatively unchanged upon binding to a guest molecule, unlike non-rigid hosts where the host's structure can undergo changes when interacting with guest molecules. As a positively charged hydrophobic guest, berberine is well-suited for interacting with NaDC aggregates. The absence of a spectral shift between free berberine and berberine bound to the NaDC aggregates (Figure 2.2 (b)) indicates that berberine does bind within the hydrophobic primary aggregates but binds to the aggregates through electrostatic interactions between the cationic nitrogen of berberine and carboxylate groups of NaDC, which are ionized at the pH of water used for this work. If berberine was bound inside of the NaDC primary aggregates, a change in the maximum emission wavelength would be expected due to the change in the microenvironment's polarity from bulk water to the more hydrophobic site in primary aggregates.[14] Adding NaDC to solutions

containing the berberine@CB[7] complex led to changes in steady-state fluorescence emission spectra maxima and quantum yield of berberine (Figures 2.11). The shift in the steady-state fluorescence emission spectra of berberine shows that the presence of NaDC aggregates causes a relocation of berberine from complexation with CB[7] to the binding with NaDC aggregates. At lower concentrations of NaDC, primary aggregates are present. By increasing the NaDC concentration, secondary aggregates begin to form with the association of primary aggregates. In both concentration ranges where primary and secondary aggregates exist, berberine shows an emission, providing evidence of its binding to both primary and secondary aggregates. The concentration of NaDC molecules at which NaDC primary aggregates begin to form is at least 5000 times higher than the concentration of CB[7]. Hence, the high concentration of NaDC may prevail over the relatively high binding affinity ($K_{eq} = (5.3 \pm 0.7) \times 10^7$ M^{-1} at 283 K)[32] between berberine and CB[7], making the binding between berberine and NaDC primary and secondary aggregates the dominant interaction.[24] This finding shows that even with a strong binding affinity between berberine and CB[7], it is not the only factor determining the binding efficiency between them when other binding sites are available. Differences in the quantity of binding sites between two host molecules can lead to alternative weak interactions with more binding sites superseding high binding affinity of the stronger host-guest interactions. Therefore, studying all possible interactions between the components of a supramolecular system will enable the prediction of the final supramolecular systems formed by individual molecules.

NaDC aggregates also affect the dynamics between berberine and CB[7], due to the formation of primary and secondary NaDC aggregates in the solution phase. Berberine binds to the NaDC aggregates, as evidenced by differences in amplitudes when mixing berberine and various NaDC concentrations and an increase in the berberine's fluorescence emission intensity (Figures 2.2 and 2.14). Through steady-state fluorescence and kinetic experiments, it was found that the dissociation and association of berberine from NaDC could not be detected under the current experimental conditions, as the kinetics of association and dissociation occur more rapidly than the resolution of the equipment allows. For future studies, laser temperature jump could be used as a technique to analyze the dissociation and association of berberine from NaDC. This technique involves rapidly heating the sample with a laser pulse, causing a sudden temperature increase. The system's response to this thermal perturbation can then be monitored as it relaxes back to equilibrium.

Reaching the new equilibrium faster than the resolution of the equipment is considered as a dead time of the instrument (Figure 2.14 (a, b)). Also, the concentration of Ada^+ at 40 μM was shown not to displace berberine bound to NaDC aggregates as the emission intensity of berberine did not decrease upon addition of 40 μM Ada^+ (Figure 2.12). Hence, when both CB[7] and NaDC are present in the system with berberine, only the kinetics for the berberine@CB[7] was observed in the stopped flow kinetic experiments.

$$B^+@CB[7] \leftrightarrows B^+ + CB[7]$$ **Equation 2.3**

A previous literature report showed that the values of both k_+ and k_- for berberine with CB[7] (Equation 2.3) are affected by changes in temperature and the salt concentration of the solution; however, these dependencies are not explicitly represented in the equation.[32] Consequently, a constant temperature and sodium cation concentration was maintained in my studies.

$$CB[7] + Ada^+ \rightleftarrows Ada^+@CB[7]$$ **Equation 2.4**

Following the formation of the berberine complex with CB[7] and its dissociation, addition of Ada^+ will lead to the complexation of CB[7] with Ada^+ (Equation 2.4). If the concentration of Ada^+ is in a range in which the rate of the association of Ada^+ to CB[7] is higher than the reassociation of berberine to CB[7], Ada^+ will prevent the reassembly of the berberine and CB[7] complex, as Ada^+ will enter to the cavity of CB[7] in a very fast process and hence, the only process that will be observed is the dissociation of berberine from CB[7] in the presence of excess Ada^+.

$$B^+@CB[7] \rightarrow B^+ + CB[7]$$ **Equation 2.5**

$$B^+@CB[7] \cdot Na^+ \rightarrow B^+ + CB[7] \cdot Na^+$$ **Equation 2.6**

$$k_{obs} = k_{app-}$$ **Equation 2.7**

In the literature, it has been mentioned that the presence of salts can form a ternary complex between CB[7], berberine, and the cation (Equation 2.6).[33] Hence, in the solution, there will be two different types of complexes: one with berberine and CB[7], and another with berberine, CB[7], and the cation. Hence, both the dissociation of berberine from CB[7] and from CB[7] with cation contribute to the observed rate constant, which is equivalent to the apparent

dissociation rate constant. The apparent dissociation constant is a function of the dissociation of berberine from CB[7] both with and without cation.

The presence of varying concentrations of NaDC monomers did not affect the dissociation rate constant of berberine from the berberine@CB[7] complex. Upon increasing the concentration of NaDC and the formation of primary aggregates (5 mM NaDC), the observed rate constant increased. With further increase in the NaDC concentration and the formation of secondary aggregates (12–25 mM NaDC), the increase in k_{obs} continued. This increase in k_{obs} displays a linear relationship within the range of 5 to 25 mM NaDC, which corresponds to the presence of both primary and secondary aggregates. Formation of secondary aggregates does not lead to a different observed rate constant change compared to primary aggregates (Figure 2.17 (b)). At higher concentrations of Ada^+ (80 μM) the trend is not continuous and there is not a relationship between the formation of aggregates and the values of k_{obs} (Figure 2.18 (b)). This might happen because Ada^+ could replace berberine in NaDC aggregates, leading to a more complex process.

One possible mechanism for the acceleration of k_{obs} upon addition of NaDC to berberine complexed with CB[7] with and without cation is that the complex may relocate from bulk water to aggregates. The increased likelihood of Ada^+ encountering the complex and displacing berberine within CB[7] is attributed to the electrostatic interaction between the positively charged Ada^+ and the negative charge of NaDC aggregates. Through the relocation of the berberine@CB[7] complex from bulk water to NaDC aggregates and the electrostatic interaction between Ada^+ and the NaDC aggregates increases the possibility of Ada^+ being present in the NaDC primary and secondary aggregates, which facilitates the encounter of Ada^+ with the berberine@CB[7] complex present in the aggregates, leading to the displacement of berberine. If there were a mechanism based on the type of aggregates, it would involve the complex binding to both primary and secondary aggregates. However, since primary and secondary aggregates have different binding sites for molecules with varying hydrophilicity, any binding between the complex and aggregates would likely result in a change in the trend of the observed rate constant before and after the formation of secondary aggregates. Given that no such change in trend has been observed, it shows that the mechanism does not involve binding of the complex to the binding sites of the primary and secondary aggregates.

2.5. Conclusion

The objective of this work was to study the dissociation kinetics of a hydrophobic cationic guest (berberine) from CB[7] in the presence of different concentrations of NaDC, and studying the interaction between the guest molecule and both CB[7] and NaDC aggregates. We used changes in the fluorescence emission and UV-Vis absorption spectra of the guest molecule as indicators of these interactions. The main findings suggest that the addition of NaDC caused a shift and redistribution of the guest molecule between CB[7] and NaDC aggregates, indicating an interaction with both hosts. It was also shown that the dissociation of berberine from the complex with CB[7] changes upon the addition of NaDC primary and secondary aggregates to the system, but there is no change in the presence of NaDC monomers. The relocation of the guest and CB[7] complex from bulk water to the NaDC aggregates might explain this phenomenon. By achieving the objective of this work, we concluded that simply adding a host to a supramolecular system without studying the interaction of each component with each other makes it difficult to predict the outcome.

In drug delivery systems, while the primary focus often lies on the equilibrium constant between the drug and the delivery system, the crucial factor, after the drug reaches the body and is distributed in the bloodstream, is the drug's dissociation from the carrier into the surrounding medium. Hence, studying the parameters affecting the dissociation rate constant of guests from hosts is important for designing functional controlled delivery systems.

2.6. References

(1) Assaf, K. I.; Nau, W. M. Cucurbiturils: From Synthesis to High-Affinity Binding and Catalysis. *Chem. Soc. Rev.* **2015**, *44*, 394-418.
(2) Masson, E.; Ling, X.; Joseph, R.; Kyeremeh-Mensah, L.; Lu, X. Cucurbituril Chemistry: A Tale of Supramolecular Success. *RSC Adv.* **2012**, *2*, 1213-1247.
(3) Moghaddam, S.; Yang, C.; Rekharsky, M.; Ko, Y. H.; Kim, K.; Inoue, Y.; Gilson, M. K. New Ultrahigh Affinity Host−Guest Complexes of Cucurbit[7]uril with Bicyclo[2.2.2]octane and Adamantane Guests: Thermodynamic Analysis and Evaluation of M2 Affinity Calculations. *J. Am. Chem. Soc.* **2011**, *133*, 3570-3581.
(4) Bohne, C. Supramolecular Dynamics. *Chem. Soc. Rev.* **2014**, *43*, 4037-4050.
(5) Weiser, J. R.; Saltzman, W. M. Controlled Release for Local Delivery of Drugs: Barriers and Models. *J. Control. Release.* **2014**, *190*, 664-673.
(6) Vos, K. A. A. Systems Chemistry Approach to Understanding Cucurbit[7]uril-guest Dynamics. PhD University of Victoria, 2020. http://hdl.handle.net/1828/11797.
(7) Thomas, S. S.; Tang, H.; Bohne, C. Noninnocent Role of Na^+ Ions in the Binding of the N-Phenyl-2-naphthylammonium Cation as a Ditopic Guest with Cucurbit[7]uril. *J. Am. Chem. Soc.* **2019**, *141*, 9645-9654.
(8) Garidel, P.; Hildebrand, A.; Knauf, K.; Blume, A. Membranolytic Activity of Bile Salts: Influence of Biological Membrane Properties and Composition. *Molecules* **2007**, *12*, 2292-2326.
(9) Sobotka, H.; Czeczowiczka, N. The Gelation of Bile Salt Solutions. *J. Colloid Sci.* **1958**, *13*, 188-191.
(10) Jover, A.; Troncoso, J.; di Gregorio, M. C.; Fraga López, F. Thermodynamic Properties of Sodium Deoxycholate at the Gel-Sol Transition. *J. Mol. Liq.* **2022**, *361*, 119621.
(11) Small, D. M.; Penkett, S. A.; Chapman, D. Studies on Simple and Mixed Bile Salt Micelles by Nuclear Magnetic Resonance Spectroscopy. *Biochim. Biophys. Acta, Lipids Lipid Metab.* **1969**, *176*, 178-189.
(12) Li, R.; Carpentier, E.; Newell, E. D.; Olague, L. M.; Heafey, E.; Yihwa, C.; Bohne, C. Effect of the Structure of Bile Salt Aggregates on the Binding of Aromatic Guests and the Accessibility of Anions. *Langmuir* **2009**, *25*, 13800-13808.
(13) Rinco, O.; Nolet, M.-C.; Ovans, R.; Bohne, C. Probing the Binding Dynamics to Sodium Cholate Aggregates Using Naphthalene Derivatives as Guests. *Photochem. Photobiol. Sci.* **2003**, *2*, 1140-1151.
(14) Amundson, L. L.; Li, R.; Bohne, C. Effect of the Guest Size and Shape on Its Binding Dynamics with Sodium Cholate Aggregates. *Langmuir* **2008**, *24*, 8491-8500.
(15) Niu, C. G.; Gui, X. Q.; Zeng, G. M.; Yuan, X. Z. A Ratiometric Fluorescence Sensor with Broad Dynamic Range Based on Two pH-Sensitive Fluorophores. *Analyst* **2005**, *130*, 1551-1556.
(16) Kalyanasundaram, K.; Thomas, J. K. Environmental Effects on Vibronic Band Intensities in Pyrene Monomer Fluorescence and Their Application in Studies of Micellar Systems. *J. Am. Chem. Soc.* **1977**, *99*, 2039-2044.
(17) van de Linde, S.; Aufmkolk, S.; Franke, C.; Holm, T.; Klein, T.; Löschberger, A.; Proppert, S.; Wolter, S.; Sauer, M. Investigating Cellular Structures at the Nanoscale with Organic Fluorophores. *Chem. Biol.* **2013**, *20*, 8-18.
(18) Yang, Y.; Yang, X.; Jiao, C.-X.; Yang, H.-F.; Liu, Z.-M.; Shen, G.-L.; Yu, R.-Q. Optical Sensor for Berberine Utilizing Its Intrinsic Fluorescence Enhanced by the Formation of Inclusion Complex with Butylated-β-Cyclodextrin. *Anal. Chim. Acta* **2004**, *513*, 385-392.

(19) Feng, X.; Zhang, H.; Yu, P. X-ray Fluorescence Application in Food, Feed, and Agricultural Science: A Critical Review. *Crit. Rev. Food Sci. Nutr.* **2021**, *61*, 2340-2350.
(20) Koner, A. L.; Nau, W. M. Cucurbituril Encapsulation of Fluorescent Dyes. *Supramol. Chem.* **2007**, *19*, 55-66.
(21) Mana, T.; Devi, O. B.; Singh, Y. D. Therapeutic Application of Berberine: a Consolidated Review. *Curr. Pharmacol. Rep.* **2023**, *9*, 329-340.
(22) Díaz, M. S.; Freile, M. L.; Gutiérrez, M. I. Solvent Effect on the UV/Vis Absorption and Fluorescence Spectroscopic Properties of Berberine. *Photochem. Photobiol. Sci.* **2009**, *8*, 970-974.
(23) Megyesi, M.; Biczók, L. Considerable Fluorescence Enhancement upon Supramolecular Complex Formation between Berberine and p-Sulfonated Calixarenes. *Chem. Phys. Lett.* **2006**, *424*, 71-76.
(24) Megyesi, M.; Biczók, L.; Jablonkai, I. Highly Sensitive Fluorescence Response to Inclusion Complex Formation of Berberine Alkaloid with Cucurbit[7]uril. *J. Phys. Chem. C.* **2008**, *112*, 3410-3416.
(25) Seyedalikhani, M. Exploring the Binding of Small Guest Molecules in Sodium Deoxycholate Hydrogels. PhD University of Victoria, 2016. http://hdl.handle.net/1828/7615.
(26) Li, P.; Malveau, C.; Zhu, X. X.; Wuest, J. D. Using Nuclear Magnetic Resonance Spectroscopy to Probe Hydrogels Formed by Sodium Deoxycholate. *Langmuir* **2022**, *38*, 5111-5118.
(27) Thomas, S. S. Mechanistic Diversity in the Guest Binding with Cucurbit[7]uril or Octa acid Complexes. PhD University of Victoria, 2016. http://hdl.handle.net/1828/7394.
(28) Kundu, N.; Roy, A.; Banik, D.; Sarkar, N. Unveiling the Mode of Interaction of Berberine Alkaloid in Different Supramolecular Confined Environments: Interplay of Surface Charge between Nano-Confined Charged Layer and DNA. *J. Phys. Chem. B.* **2016**, *120*, 1106-1120.
(29) Zhu, J.-J.; Zhang, J.-J.; Zhao, G.-C.; Chen, H.-Y. Study of Interaction of Berberine With DNA in the Presence of β -Cyclodextrin. *Spectrosc. Lett.* **1998**, *31*, 1705-1718.
(30) Liu, Q.; Xie, Z.; Liu, T.; Fan, J. Determination of Berberine Hydrochloride Using a Fluorimetric Method with Silica Nanoparticles as a Probe. *RSC Adv.* **2018**, *8*, 6075-6082.
(31) Sen, S.; Paul, B. K.; Guchhait, N. Differential Interaction Behaviors of an Alkaloid Drug Berberine with Various Bile Salts. *J. Colloid Interface Sci.* **2017**, *505*, 266-277.
(32) Miskolczy, Z.; Biczók, L. Kinetics and Thermodynamics of Berberine Inclusion in Cucurbit[7]uril. *J. Phys. Chem. B.* **2014**, *118*, 2499-2505.
(33) Miskolczy, Z.; Megyesi, M.; Biczók, L.; Prabodh, A.; Biedermann, F. Kinetics and Mechanism of Cation-Induced Guest Release from Cucurbit[7]uril. *Chem. Eur. J.* **2020**, *26*, 7433-7441.

Chapter 3: Characterization of NaDC hydrogels after the addition of CB[7] by fluorescence microscopy and release studies

3.1. Introduction

The interactions between components of a supramolecular system can be studied at the macroscopic, microscopic, and molecular levels. At the macroscopic level, researchers explore the bulk properties of materials. This exploration involves analyzing physical characteristics, such as solubility, viscosity, and mechanical strength, which can be tailored by controlling non-covalent interactions in the supramolecular systems.[1] On the molecular level, researchers study how individual supramolecular components interact with each other in a supramolecular system, forming unique structures. Molecular level research focuses on fundamental and mechanistic understandings of the processes and interactions of individual molecules to form supramolecular systems. This level of studies offers insights into the dynamics[2], kinetics, and thermodynamic processes involved in the formation of host-guest interactions[3] and the overall complexity of these systems. Understanding interactions between the building blocks in the supramolecular systems is a crucial step in designing functional materials, like molecular sensors or drug delivery systems. A microscopic study of supramolecular systems involves examining their structures in detail. There is no straightforward relationship that connects the microscopic, macroscopic, and molecular length scales. To understand how each individual component contributes to the overall functionality of a multi-component system like a supramolecular hydrogel, it is important to get information at different length scales.[4]

In the previous chapter, the effect of NaDC, a main component of a hydrogel, on the dissociation of a hydrophobic and cationic guest (berberine) from CB[7] was studied in aqueous solutions, which also constitutes the mobile phase of the NaDC hydrogel at the molecular level. It was shown that the presence of NaDC aggregates has an effect on the dissociation rate constant of berberine from CB[7]. This result suggests that every component within a supramolecular system has direct or indirect effects on the system's behavior at the molecular level.

Introducing a new component to a supramolecular system, in which the new component can be involved in non-covalent interactions, will change the properties of the system at different

length scales.[5] Previous studies in our group, showed that adding CB[6] changed the properties of the NaDC hydrogels in each of the three length scales. It was shown that adding CB[6] increases the mechanical strength of the NaDC hydrogel.[6] The change in the mechanical strength of NaDC after the addition of CB[6] resulted in a macroscopic-level change. Also, the presence of CB[6] in the NaDC hydrogel changed the immobilized spherical aggregates of NaDC to fibrous structures at the microscopic level. The mechanical strength and structure of the gel changed; however, the release profile of small molecules from NaDC hydrogel into the surrounding medium was affected differently, depending on the structure of the small molecule (Figure 3.1).

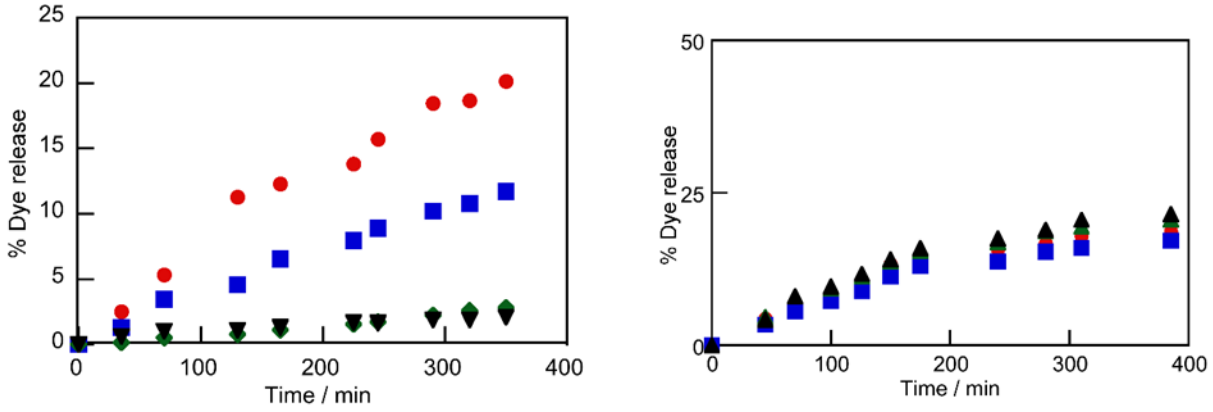

Figure 3.1. Release profiles for pyrene (5 μM, left) and for rhodamine 6G (10 μM, right) dyes from NaDC gels (50 mM) with different CB[6]/NaDC ratios: 0 (red circle), 0.05 (blue square), 0.1 (green rhombus), 0.15 (black triangle). Reprinted with permission from [Sree Gayathri Talluri, Effect of cucurbit[6]uril on the structure and dynamics of NaDC gels, University of Victoria, 2021].[7]

The release kinetics for pyrene (Chart 3.1 (b)) from the NaDC hydrogel to the surrounding medium slowed down after the addition of CB[6] (Figure 3.1 left). However, the release of rhodamine 6G (Chart 3.1 (b)) was not affected by the addition of CB[6] (Figure 3.1 (right)) although the structure of the hydrogel was the same. These data suggest that supramolecular systems can be optimized to achieve desired properties at different length scales. For example, CB[6] can be added to change the strength of the hydrogel without affecting the release of certain small molecules, such as rhodamine 6G. These results also show that pyrene

has an interaction with CB[6], whereas rhodamine 6G does not. Pyrene is a neutral and hydrophobic dye, making it a good candidate to have an interaction with the hydrophobic aggregates of NaDC.[8] Rhodamine 6G, being a cationic dye, encounters the negative charge of the NaDC aggregates, leading to a charge-charge interaction between them. Among non-covalent interactions, charge-charge interactions are more favorable compared to the hydrophobic effect. Hence, the positive charge of rhodamine 6G is the primary driving force for the interaction between the aggregates and the dye, rather than the dye's hydrophobicity. Therefore, CB[6] is presumed to be within the aggregates, which is why it changes the structure of the immobilized NaDC aggregates.

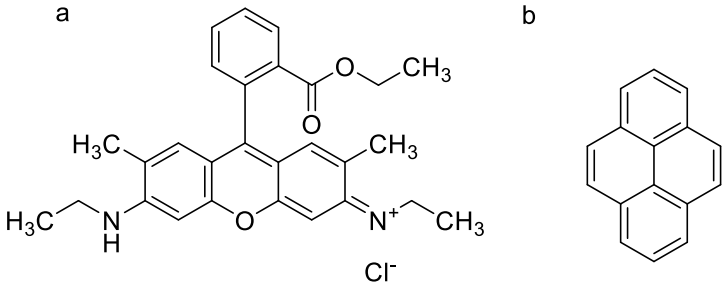

Chart 3.1. (a) Chemical structure of rhodamine 6G. (b) Chemical structure of pyrene.

In this chapter, CB[7] was added to the NaDC hydrogel because CB[7] is more soluble in water than CB[6]. My hypothesis is that a certain percentage of CB[7] will become localized in the mobile phase of the gel and interact with guests located in this portion of the hydrogel due to the higher hydrophilicity of CB[7] than CB[6]. This interaction is expected to result in a modification of the release of hydrophilic dyes from the NaDC hydrogel into the surrounding medium. Also, if the hypothesis regarding the presence of most of the CB[7] molecules in the mobile phase of the gel is correct, the gel structure of the NaDC hydrogel should be less affected with the addition of CB[7] when compared with the effect observed with the addition of CB[6].

3.1.1. Objective

The objective of this work is to study how the addition of CB[7] affects the structure of NaDC hydrogels and its impact on the release of rhodamine 6G from the hydrogel into the surrounding medium. For this aim, a confocal laser scanning microscope (CLSM) was used to obtain structural information, and release studies were done by using the static diffusion method.

3.2. Experimental section

3.2.1. Materials

CB[6] and CB[7] were synthesized and purified by standard protocols in the Bohne group.[9] Berberine chloride (Sigma-Aldrich, 98 %), methanol (Fisher, spectral grade, ≥ 99.9%), deionized water (Barnstead NANOpure deionizing systems, ≥ 17.8 MΩ cm^{-1}), NaDC (Fluka, > 98%), NaH_2PO_4 (Anachemia, > 98%), Na_2HPO_4 (Anachemia, > 98%), rhodamine 6G (Sigma Aldrich, 99%) were used as received.

3.2.2. Sample preparation

For all hydrogels for microscope and release studies, the samples were made in 3-dram sample vials. Stock solutions of NaDC (0.2 M) were prepared in deionized water and the solutions were heated for 15 min at a temperature of 60 °C in a water bath. Stock solutions of rhodamine 6G (0.5 mM) were prepared by adding 0.23 mg rhodamine 6G to 1 mL spectroscopic grade methanol. Stock solutions of NaH_2PO_4 (0.5 M, 1.49 g) and Na_2HPO_4 (0.5 M, 1.77 g) were prepared in deionized water and the salts were dissolved by sonicating for 30 s using a sonicator. Buffer solutions (pH = 6.50 ± 0.01) were prepared by mixing the appropriate amount of NaH_2PO_4 and Na_2HPO_4 salts.

For microscope studies, solid CB[6] or CB[7] were added to the 3-dram sample vials. Buffer and deionized water were transferred to the sample vial by using an Eppendorf pipette. The sample vials were sonicated for around 30 s in the sonicator and heated for 15 min at a temperature of 60 °C in the water bath. After 15 min, 2 μM of the selected dye and 50 mM NaDC were added to the sample vial, and the sample vials were heated for another 15 min at a temperature of 60 °C in the water bath. The gaskets and coverslips for microscope experiments were prepared and rinsed with deionized water and methanol and dried before using. Approximately 150 μL of the gel was transferred to the gasket immediately after the heating process using a 200 μL Eppendorf. A glass coverslip was carefully positioned on the side of the gasket that was open to prevent drying the sample. After the heating process, the gels were rested for 20–24 h. Berberine and rhodamine 6G concentrations were 2 μM. For CB[6]/NaDC samples, the CB[6] concentration was kept at 7.5 mM and for CB[7]/NaDC hydrogels, final

concentrations of CB[7] were 5.5 and 7.5 mM, respectively. The final volume of the samples was 500 μL.

For release studies, the CB[7]/NaDC hydrogels were made by adding CB[7], buffer solution, and deionized water to the sample vial. This solution was sonicated for around 30 s in a sonicator to ensure the CB[7] is dissolved. Then the solution was heated for 15 min at 60 °C in a water bath. While the solution was hot, appropriate amounts of rhodamine 6G and NaDC were added to the sample vial. The sample vial was then heated another 15 min at 60 °C. CB[6]/NaDC samples were prepared using the same procedure as CB[7]/NaDC, with the only difference of addition of CB[6] instead of CB[7]. The concentrations of CB[6] in CB[6]/NaDC hydrogels and CB[7] for CB[7]/NaDC hydrogels were 5 mM. The concentrations of NaDC and buffer for all gels were 50 mM. The final volume of the samples was 3000 μL. An amount of 2000 μL sample was transferred to a triangular cell and rested for 20 h.

3.2.3. Instrumentation

3.2.3.1. CLSM experiments

The microscope experiments were done using a Zeiss LSM 880 microscope and the system was set to a 20× long working distance (LWD) and 63× oil lens. Rhodamine 6G was excited with a 488 nm laser and the emission was collected between 515 and 570 nm. Berberine was excited at 405 nm and the emission was collected between 480 and 650 nm. The intensity of the laser was set to 20%. The pinhole diameter was adjusted to 1 Airy Unit (AU) and the detector gain was adjusted between 600 and 800 V. Images were captured using the software's recommended pixel size and with a pixel depth of 12 bits. The temperature was the room temperature. The measurements were done at a depth of 50–100 μm from the surface of the gasket. Features that are shown in microscope studies are related to immobilized aggregates and mobile aggregates are shown as the background of the images.

3.2.3.2. Release experiments by steady-state fluorescence

Release studies were conducted using the static diffusion method.[10] In this method, the release medium is placed above the surface of the gel. To track the release of the dye from the gel, aliquots from the release medium were periodically collected, and the amount of analyte was analyzed using steady-state fluorescence measurements. Fluorescence emission spectra were collected using a 10 × 10 mm quartz cuvette cell on a PTI QM-40 spectrophotometer. The excitation wavelength was 480 nm and the wavelength range for the detection of the emission was 490–700 nm. The step size was 0.5 nm, the integration time was set to 0.25 s and the excitation and emission monochromator bandwidths were 2 nm. The integrated area was measured between 530-580 nm.

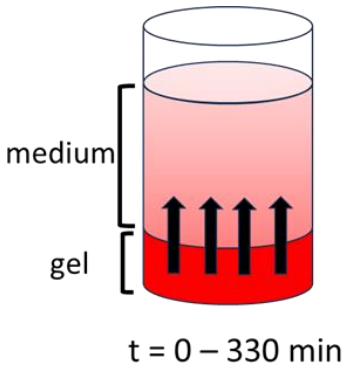

Scheme 3.1. Schematic representation of the static diffusion method for release studies.

The medium is a 50 mM phosphate buffer (pH = 6.50 ± 0.01) added to the top of the gel after a 20 h resting period (Scheme 3.1). The integrated area for the fluorescence of the fluorophore was analyzed using steady-state fluorescence. A calibration curve for rhodamine 6G in buffer was established by adding 2 μL of rhodamine 6G stock solution to the phosphate buffer in the quartz cell for each measurement. The percentage of the released dye was calculated by comparing the moles of the dye in the released medium and in the gel structure by using the linear equation obtained from the calibration curve of the dye in the medium.

3.2.4. Effect of CB[6] on the morphology of the NaDC hydrogel

Previous studies in the Bohne research group have shown that the presence of CB[6] as an additive in the NaDC hydrogels led to a transition from spherical aggregates within the immobile phase to fibrous structures.[7] Additionally, rheology studies suggested that the presence of CB[6] enhances the strength of the NaDC hydrogel.[6] Also these results suggest that CB[6] is incorporated into the gel during its formation. The low solubility of CB[6] in water can explain this phenomenon, as CB[6] tends to prefer staying within the gel phase which has a higher hydrophobicity compared to the mobile phase of the gel. CLSM can image the immobile structure of the gel, but this technique does not image NaDC aggregates that are freely moving because of their fast diffusion.

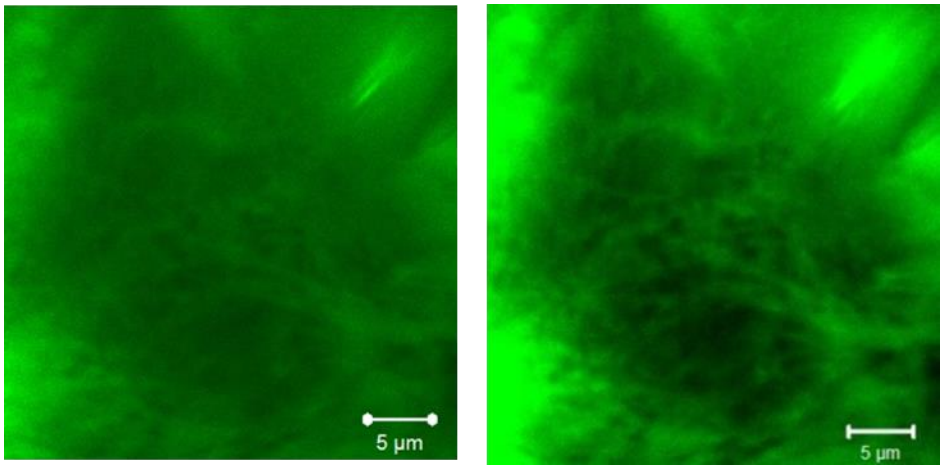

Figure 3.2. Confocal images of CB[6]/NaDC with a ratio of 0.15 gel tagged with rhodamine 6G. The right and left panels represent the same region of the sample, captured at different focal planes.

In previous studies, CB[6] was incorporated as an additive into NaDC hydrogel. Prior to starting work on NaDC hydrogels modified with CB[7], the same experiment involving CB[6]/NaDC with a ratio of 0.15 was repeated. The aim of this experiment was to compare the results and assess their reproducibility. CLSM results obtained in the presence of CB[6] within NaDC hydrogel showed that the presence of CB[6] changes the structure of NaDC spherical aggregates inside immobile phase of the gel, transforming them into fibrous structures (Figure 3.2). The transformation of spherical aggregates to a fibrous structure was not reproducible

compared to previous work. While fibrous structures were observed, they differed from those reported by Talluri.[7]

3.3. Results

3.3.1. Optimizing the CB[7] concentration for NaDC hydrogel formation

For the CB[6]/NaDC hydrogel, the CB[6] concentration was adjusted to the highest level at which the most significant structural changes in the NaDC hydrogel were observed. For the CB[7]/NaDC hydrogel, I began by adding the same concentration as I did for CB[6]. However, adding CB[7] at the highest amount achievable for CB[6] caused precipitation inside of hydrogel (Figure 3.3 (a)). The CB[7]/NaDC ratio was reduced to 0.12 to achieve a hydrogel without precipitation. However, even at this ratio of CB[7] to NaDC, white spots were visible to the naked eye in the hydrogel (Figure 3.3 (b)). Reducing the concentration of CB[7] to achieve a molar ratio of 0.11 for CB[7] to NaDC resulted in the formation of a hydrogel without any visible precipitation (Figure 3.3 (c)).

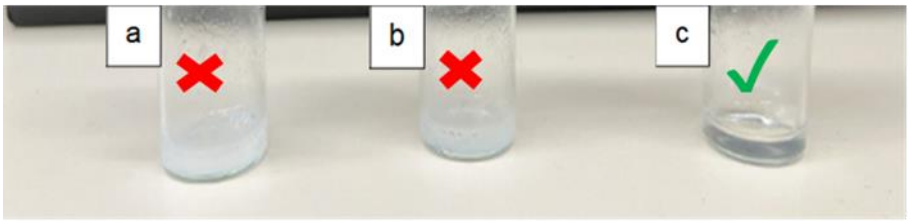

Figure 3.3. NaDC/CB[7] hydrogels with NaDC/CB[7] ratios of (a) 0.15 (b) 0.12 (c) 0.11.

3.3.2 CLSM images of dyes with an NaDC/CB[7] ratio of 0.11

For CLSM experiments, different dyes were used in the hydrogel based on the dye's characteristics. Rhodamine 6G is a hydrophilic dye[11] capable of forming a 1:1 complex with CB[7].[12] Also, rhodamine 6G's hydrophilic nature enables it to remain in the mobile phase of the gel. In contrast, berberine chloride is hydrophobic, and the expectation is that it would prefer to localize within the immobile aggregates rather than in the mobile phase. Berberine also binds to the CB[7] cavity in a 1:1 ratio, primarily driven by the hydrophobic effect.[13]

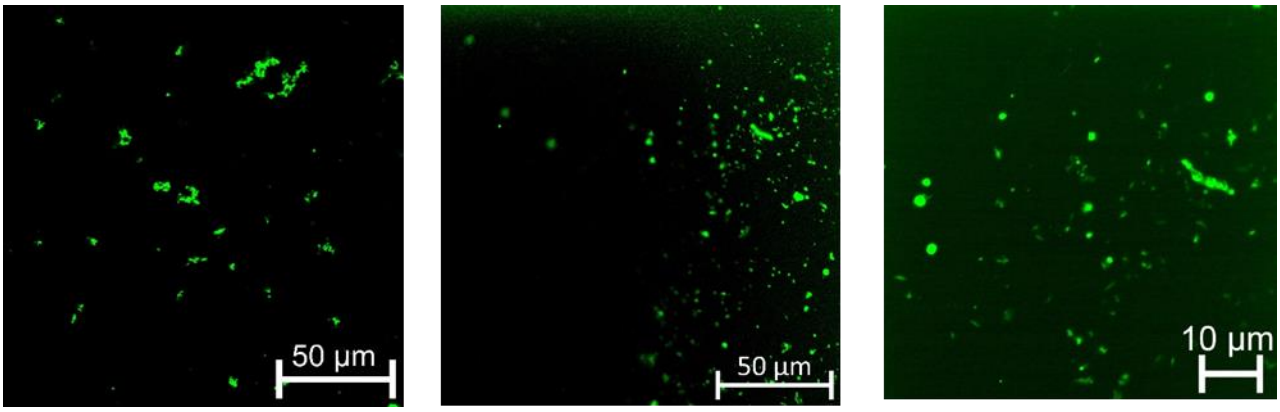

Figure 3.4. Confocal images of NaDC/CB[7] gel tagged with rhodamine 6G at an CB[7]/NaDC ratio of 0.11. All panels correspond to a same sample.

NaDC hydrogels consist of spherical aggregates within their structure.[7] When CB[7] is added into NaDC hydrogels (Figure 3.4) containing the rhodamine 6G dye, it causes elongation of the spherical aggregates characteristic of the gel in the absence of CB[*n*]s. The observation of the elongated aggregates within the gel structure suggests that rhodamine 6G interacts with the immobilized NaDC aggregates. This shift in aggregate shape signifies that CB[7] is integrating into the hydrogel structure, although it does not induce the formation of fibrous structures like CB[6] does.

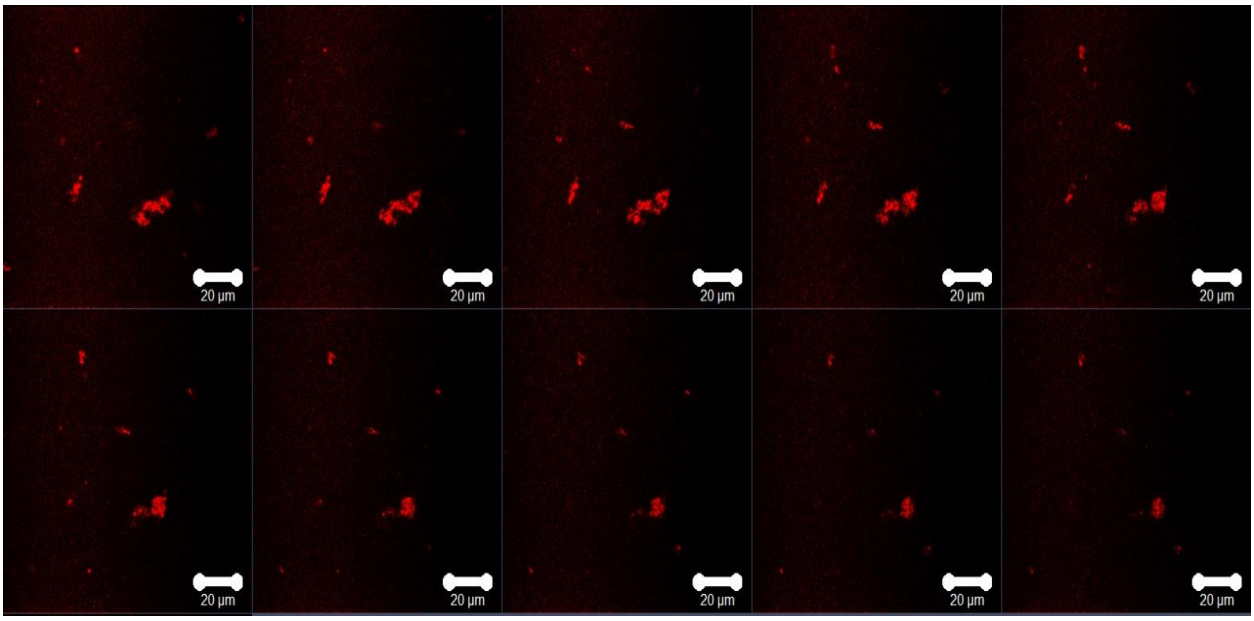

Figure 3.5. Confocal images of NaDC/CB[7] gel tagged with berberine at CB[7]/NaDC ratio of 0.11 in different depths (Z = 102–302 μm) of hydrogel. The scale bars correspond to 20 μm.

Monitoring the changes in different depths of the hydrogel tagged with berberine chloride shows that the dispersion of the aggregates in a 3-D network (Figure 3.5). Figure 3.5 shows that the dispersion of aggregates forming the immobile phase within the hydrogel is heterogeneous. More heterogeneity and nonuniformity in the distribution of these aggregates in the solid network of the hydrogel corresponds to a weaker mechanical strength compared to hydrogels with uniformly dispersed aggregates or micelles.[14] Comparing the CLSM images of CB[7]/NaDC hydrogels tagged with rhodamine 6G appear to show more aggregates compared to those tagged with berberine.

Also, it was easier to identify immobilized aggregates in hydrogels with rhodamine 6G compared to gels tagged with berberine.

3.3.3. Confocal images of dyes with NaDC/CB[7] ratio of 0.15

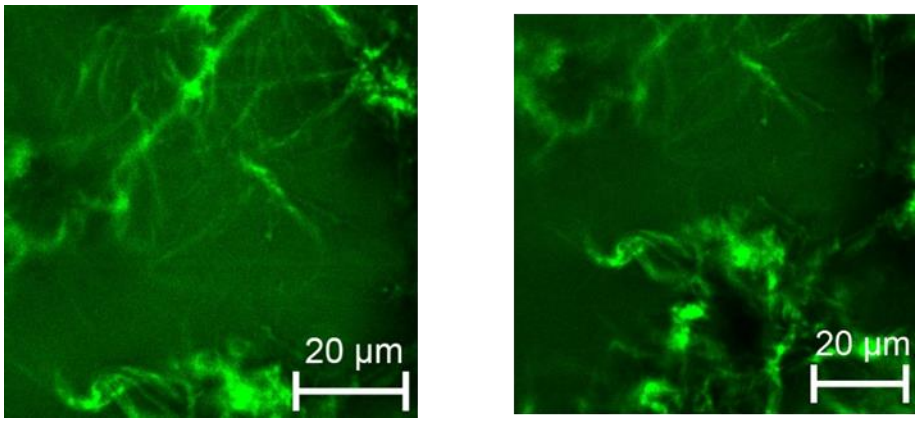

Figure 3.6. Confocal images of NaDC/CB[7] gel tagged with rhodamine 6G at CB[7]/NaDC ratio of 0.15. Both panels correspond to a same sample.

Increasing the concentration of CB[7] to a point where visible solid particles start to appear has resulted in a change in the structure of the NaDC hydrogel (Figure 3.6). The nature of these particles differ from the fibrous structures observed in the CB[6] and NaDC hydrogel, as the CB[7]-related structures are larger in size. These fibrous structures are also present in the CB[7]/NaDC hydrogels tagged with berberine (Figure 3.7).

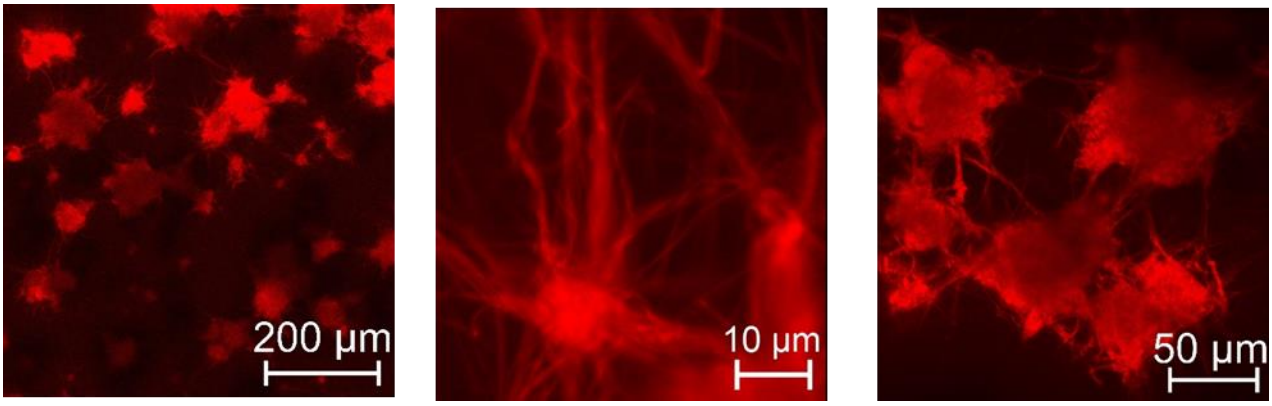

Figure 3.7. Confocal images of NaDC/CB[7] gels tagged with berberine at CB[7]/NaDC ratio of 0.15 ([NaDC] = 50 mM). All panels correspond to a same sample.

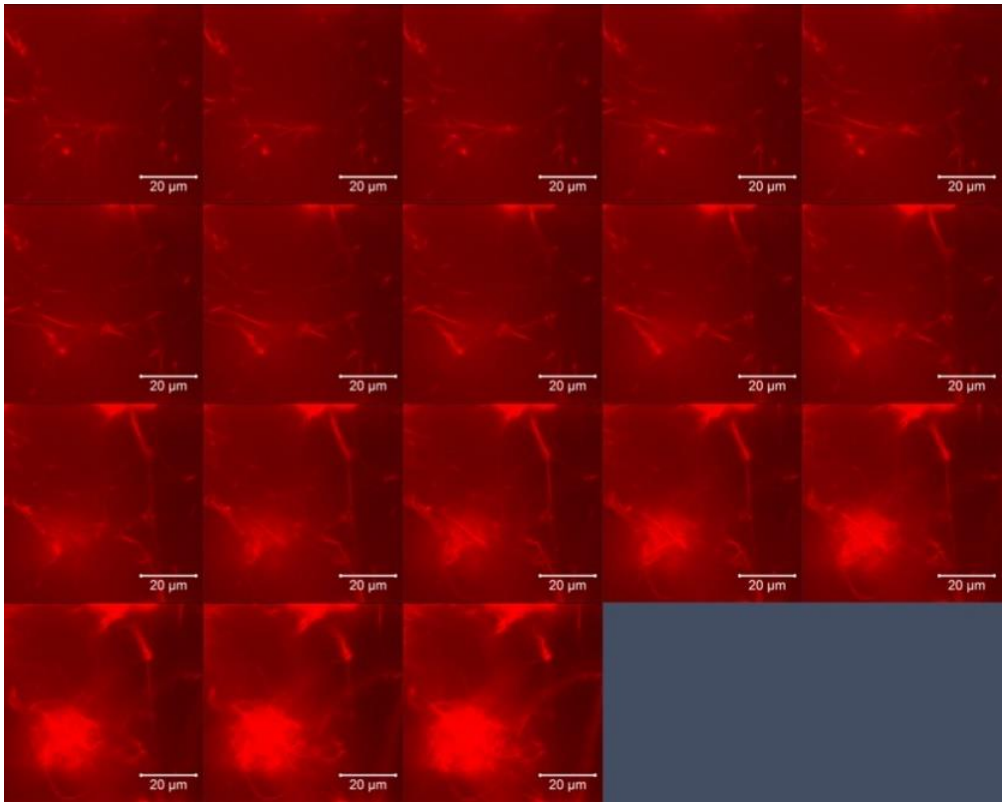

Figure 3.8. Confocal images of NaDC/CB[7] gel tagged with berberine at CB[7]/NaDC ratio of 0.15 in different depth (Z = 54–234 μm) of hydrogel. The scale bars correspond to 20 μM.

The presence of particles in different depths of the hydrogel shows that the hydrogel has formed particles that have dispersed heterogeneously throughout the sample (Figure 3.8)

3.3.4. Release studies

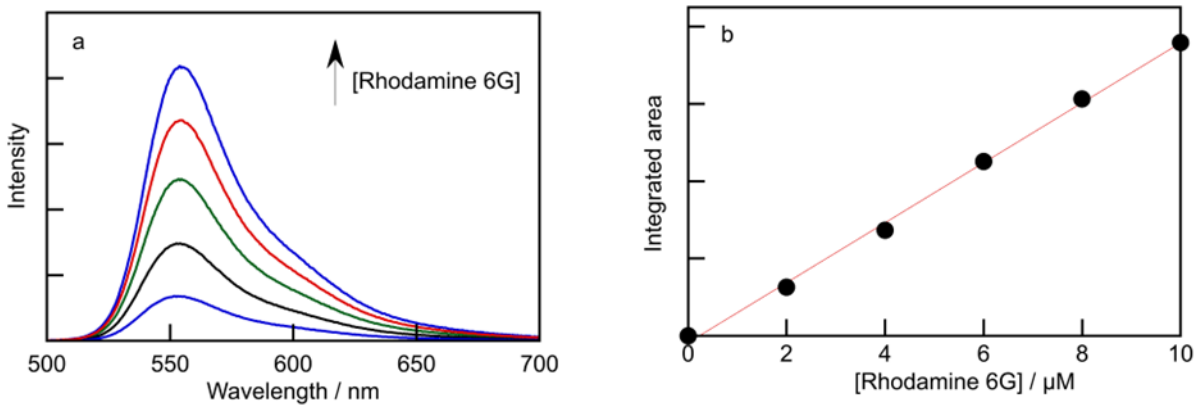

Figure 3.9. (a) Steady-state fluorescence emission spectra of known concentrations of rhodamine 6G (λ_{ex} = 480 nm) in phosphate buffer used to establish the calibration curve. (b) Calibration curve derived from the data in panel (a).

To determine the concentrations of the dye that have been released from the hydrogel, a calibration curve was required (Figure 3.9 (b)). This calibration curve was constructed by measuring the integrated area of the emission fluorescence spectra of known concentrations of rhodamine 6G (Figure 3.9 (a)). This analytical approach allowed for the quantification of the released dye's concentration into the surrounding medium.

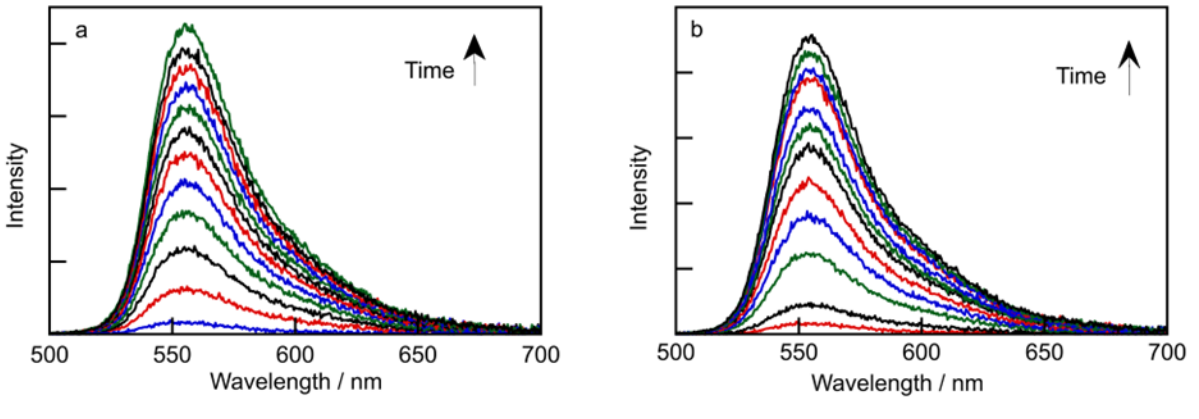

Figure 3.10. (a) Steady-state fluorescence emission spectra of the surrounding medium collected at different times during the release of 10 μM rhodamine 6G (λ_{ex} = 480 nm) from (a) NaDC/CB[6] ([NaDC] = 50 mM, CB[6] = 5 mM) and (b) NaDC/CB[7] ([NaDC] = 50 mM, CB[7] = 5 mM) hydrogels. Data was obtained between 0–330 min.

Over time, the amount of dye being released from the hydrogel into the medium added to the top of the gel is increasing, as shown by the higher fluorescence intensity of the medium. This increase is attributed to the difference in the concentration of rhodamine 6G between the hydrogel and the medium. The increase in the percentage of the dye being released, is indicated by the rising intensity of the steady-state fluorescence emission (Figure 3.10).

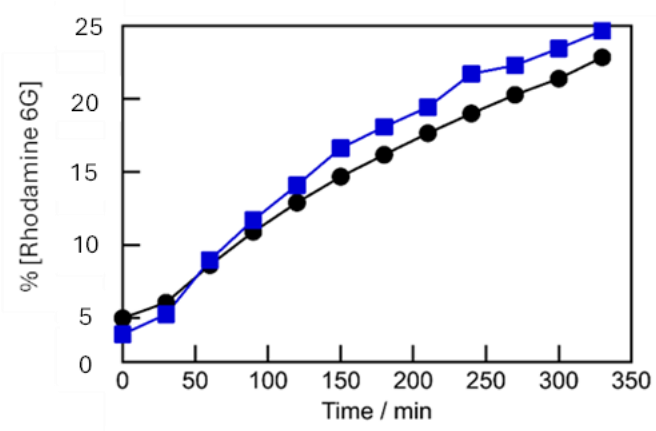

Figure 3.11. Release profile of 10 μM rhodamine 6G from (a) NaDC/CB[6] ([NaDC] = 50 mM, [CB[6]] = 5 mM, circle,black) and (b) NaDC/CB[7] ([NaDC] = 50 mM, [CB[7]] = 5 mM, square, blue) hydrogels. Lines are drawn to guide the eye.

Figure 3.11 shows the release of rhodamine 6G from the NaDC hydrogel after the addition of CB[6] or CB[7]. There is not a significant change upon addition of CB[7] or CB[6] to the NaDC hydrogel on the release of rhodamine 6G to the surrounding medium.

3.4. Discussion

Adding additives is one way to change and modify the properties of hydrogels.[15] Supramolecular hydrogels can be modified to have different functionalities due to the reversible non-covalent bonds in their structure. CB[7] was added as an additive to NaDC supramolecular hydrogels, and the structure of the hydrogel at the microscopic length scale and the molecular-level release of small molecules from the hydrogel into the surrounding medium was observed. The effect of adding CB[7] was compared to the effect of presence of CB[6] on the structure and release of rhodamine 6G from NaDC hydrogel to the surrounding medium. CB[6] has a smaller cavity size and is more hydrophobic compared to CB[7], and the expectation was that the localization of CB[6] and CB[7] would be different inside the hydrogel due to the heterogeneity and the presence of different microenvironments with varying hydrophobicity inside the NaDC hydrogel. The initial experiments served as a preliminary step towards a larger goal, which involved incorporating both CB[6] and CB[7] into a NaDC hydrogel. The distinct localization of CB[6] within the immobile gel and CB[7] between the immobile and mobile phases could result in different functions for each host molecule. CB[6] could be used to modulate the release of the

guest molecule, while CB[7] could serve as a carrier, transporting the guest molecule from the hydrogel to the surrounding medium.

It was observed that adding CB[7] to the NaDC hydrogel changed the gel differently compared to CB[6] (Figure 3.3 (a)). There are two possible explanations for this phenomenon. One possibility is that CB[7] tends to localize more within the mobile phase due to its higher water solubility. Also, CB[7] can form a relatively weak complex with NaDC.[16] During the cooling stage of gel formation, the solubility of this complex may begin to decrease, leading to the precipitation of the CB[7] and NaDC complex. Based on the literature, the equilibrium constant of the CB[7] complexed with NaDC does not have a significant difference by changes in temperature (15 to 55 °C) and hence, the likelihood that the observed particles are consist of a NaDC monomer and CB[7] complex after gel formation is low.[16] In comparison, the CB[7] is more hydrophilic than CB[6] and the possibility for CB[7] to be incorporated into the gel structure might be lower. Consequently, as the temperature decreases and gel formation begins, CB[7] crystals might be shown as visible particles in the gel. CLSM images showed that adding the highest amount of CB[7], with no visible particles in the hydrogel, changed the shape of the NaDC immobile aggregates, making them appear elongated (Figure 3.4). This change for the addition of CB[6] to the NaDC hydrogel resulted in a transformation of immobilized aggregates into a fibrous structure (Figure 3.2). The higher solubility of CB[7] in water allows it to distribute between the mobilized and immobilized phases of the hydrogel, resulting in less incorporation into the gel's immobilized structure. The CLSM results for CB[6]/NaDC and CB[7]/NaDC hydrogels show that the localization of these structurally similar hosts (CB[6] and CB[7]) is different. The presence of CB[6] within the immobile phase of the NaDC hydrogel changed the release profile of hydrophobic and neutral dye, pyrene. On the other hand, CB[7] could act as a carrier, affecting the rate of dissociation of these dyes from the immobile phase to the surrounding medium. This distinct behavior indicates that in supramolecular hydrogels, even small changes in the structure of a newly introduced component have a significant impact on the final structure and localization of that component within the system. The qualitative analysis of the aggregates in the microscope showed that hydrogels tagged with rhodamine 6G showed more aggregates than those tagged with berberine (Figure 3.4, 3.5). The optimal distribution for rhodamine 6G, a hydrophilic and cationic dye, is to bind to the external of the negatively charged aggregates between the mobile phase and immobilized aggregates. Consequently, most of the

rhodamine 6G molecules are visible under the microscope. In contrast, for berberine, a hydrophobic and cationic dye, the best location inside the hydrogel is within the mobile and immobile aggregates, which constitute the hydrophobic portions of the hydrogel. The portion of berberine bound to immobilized aggregates can also be observed under the microscope. However, the remaining portion which of the berberine molecules will appear as background bound to mobile aggregates. Mobile aggregates constitute approximately 40% of the total aggregates.[17] For the CB[7]/NaDC hydrogel with visible particles, fibrous structures were observed. These structures were heterogeneous and did not form a well-defined 3-D network (Figure 3.8). The nature of these particles is still unknown. NMR studies on the particles can help in understanding whether the particles consist solely of CB[7] or if they are CB[7] complexed with NaDC monomers by the control experiments of NaDC monomers and also CB[7].

The next step was to see if CB[7] changes the release of small molecules from hydrogel to the surrounding medium. The hypothesis was that if the small molecules would have any interaction with CB[7], the presence of CB[7] in the NaDC hydrogel must make its release slower or faster compare with the results obtained by the presence of CB[6] in the NaDC hydrogel. Rhodamine 6G was selected as the molecule for monitoring the release. Surprisingly, it was observed that adding CB[6] and CB[7] resulted in the very similar release profile for rhodamine 6G (Figure 3.11). The initial expectation was that the interaction between CB[6] or CB[7] would change the release of the rhodamine 6G from hydrogel to the surrounding medium. However, this did not occur. The phenomenon can be explained by the fact that rhodamine 6G is cationic, while the NaDC aggregates have a negative charge in their structure. As a result, there is a possibility of a charge-charge interaction between the NaDC aggregates and rhodamine 6G. This interaction is highly likely due to the significantly higher concentration of NaDC compared to CB[6] or CB[7], which is approximately ten times greater, making the NaDC aggregates and rhodamine 6G interaction the predominant interaction. To induce a change in the release of a dye upon the addition of CB[7] to the NaDC hydrogel, the dye should have a neutral charge instead of being cationic. The neutral charge of the dye prevents interactions between the aggregates and the dye, allowing the dye to interact and form a complex with added hosts such as CB[7] and CB[6].

3.5. Conclusion

CB[7], a member of CB[*n*] family was used as an additive in the NaDC hydrogel. CB[7] is in an equilibrium, residing both within the NaDC immobilized aggregates inside the gel structure and also in the surrounding mobile phase. This equilibrium is crucial for understanding the dynamics of the system and the interactions between the components. The release of a cationic and hydrophilic dye when CB[7] is introduced into the hydrogel was measured. Despite a binding affinity of the cationic dye to CB[7], the addition of CB[7] to the hydrogel does not result in any discernible change in the release of the dye from the gel. This observation shows the importance of considering all the interactions taking place within the hydrogel and signifies that the presence of a host molecule (CB[7]) and a cationic guest molecule in a supramolecular system does not guarantee their interaction or a desired outcome. The complexity of the release mechanism is not solely determined by the overall structure of the hydrogel but extends to the molecular-level interactions between the dye and the building blocks constituting the hydrogel. The choice of drug delivery system must be thoughtfully tailored based on the unique characteristics of the guest molecule, such as its charge and other physicochemical properties.

To achieve effective drug delivery, it is essential to understand the interaction between the components at both macroscopic and microscopic levels which needs a comprehensive approach when designing drug delivery systems, ensuring that they are optimized for the specific properties and behaviors of the molecules involved, ultimately leading to successful and controlled drug release.

3.6. References

(1) Yu, G.; Yan, X.; Han, C.; Huang, F. Characterization of Supramolecular Gels. *Chem. Soc. Rev.* **2013**, *42*, 6697-6722.
(2) Bohne, C. Supramolecular Dynamics. *Chem. Soc. Rev.* **2014**, *43*, 4037-4050.
(3) D'Aria, F.; Pagano, B.; Giancola, C. Thermodynamic Properties of Hydroxypropyl-β-Cyclodextrin/Guest Interaction: A Survey of Recent Studies. *J. Therm. Anal. Calorim.* **2022**, *147*, 4889-4897.
(4) Raeburn, J.; Adams, D. J. Multicomponent Low Molecular Weight Gelators. *Chem. Commun.* **2015**, *51*, 5170-5180.
(5) Hendricks, M. P.; Sato, K.; Palmer, L. C.; Stupp, S. I. Supramolecular Assembly of Peptide Amphiphiles. *Acc. Chem. Res.* **2017**, *50*, 2440-2448.
(6) Seyedalikhani, M. Exploring the Binding of Small Guest Molecules in Sodium Deoxycholate Hydrogels. PhD University of Victoria, 2016. http://hdl.handle.net/1828/7615.
(7) Talluri, S. G. Effect of Cucurbit[6]uril on the Structure and Dynamics of NaDC Gels. PhD University of Victoria, 2021. http://hdl.handle.net/1828/13847.
(8) Jover, A.; Meijide, F.; Rodríguez Núñez, E.; Vázquez Tato, J.; Mosquera, M.; Rodríguez Prieto, F. Unusual Pyrene Excimer Formation during Sodium Deoxycholate Gelation. *Langmuir* **1996**, *12*, 1789-1793.
(9) Thomas, S. S. Mechanistic Diversity in the Guest Binding with Cucurbit[7]uril or Octa Acid Complexes. PhD University of Victoria, 2016. http://hdl.handle.net/1828/7394.
(10) Komatsu, H.; Matsumoto, S.; Tamaru, S.-i.; Kaneko, K.; Ikeda, M.; Hamachi, I. Supramolecular Hydrogel Exhibiting Four Basic Logic Gate Functions To Fine-Tune Substance Release. *J. Am. Chem. Soc.* **2009**, *131*, 5580-5585.
(11) Zehentbauer, F. M.; Moretto, C.; Stephen, R.; Thevar, T.; Gilchrist, J. R.; Pokrajac, D.; Richard, K. L.; Kiefer, J. Fluorescence Spectroscopy of Rhodamine 6G: Concentration and Solvent Effects. *Spectrochim. Acta A* **2014**, *121*, 147-151.
(12) Mohanty, J.; Nau, W. M. Ultrastable Rhodamine with Cucurbituril. *Angew. Chem. Int. Ed. Engl.* **2005**, *44*, 3750-3754.
(13) Megyesi, M.; Biczók, L.; Jablonkai, I. Highly Sensitive Fluorescence Response to Inclusion Complex Formation of Berberine Alkaloid with Cucurbit[7]uril. *J. Phys. Chem. C.* **2008**, *112*, 3410-3416.
(14) Tang, Q.; Sun, X.; Li, Q.; Wu, J.; Lin, J. A Simple Route to Interpenetrating Network Hydrogel with High Mechanical Strength. *J. Colloid Interface Sci.* **2009**, *339*, 45-52.
(15) Way, A. E.; Korpusik, A. B.; Dorsey, T. B.; Buerkle, L. E.; von Recum, H. A.; Rowan, S. J. Enhancing the Mechanical Properties of Guanosine-Based Supramolecular Hydrogels with Guanosine-Containing Polymers. *Macromolecules* **2014**, *47*, 1810-1818.
(16) Jana, R.; Ahmed, S. A.; Seth, D. Interaction between Cucurbit[7]uril and Bile Salts: An Isothermal Titration Calorimetry Study. *ChemistrySelect* **2022**, *7*, e202103800.
(17) Li, P.; Malveau, C.; Zhu, X. X.; Wuest, J. D. Using Nuclear Magnetic Resonance Spectroscopy to Probe Hydrogels Formed by Sodium Deoxycholate. *Langmuir* **2022**, *38*, 5111-5118.

Chapter 4: Summary

Understanding the properties of supramolecular hydrogels across different length scales is crucial for designing these systems from individual molecules. At the molecular level, understanding the interactions between the gel components and guest molecules provides information into binding mechanisms and enables the design of rational systems. At the microscopic level, studying the gel's structure and morphology helps tailor its mechanical properties. On a macroscopic scale, linking these properties allows for the development of responsive materials with tunable properties. Studying supramolecular systems involves studying their kinetic, thermodynamic, and structural aspects across different length scales, which are the three main subcategories of research in this field. Understanding these subcategories is essential for rationalizing the design of functional supramolecular systems which can serve as a specific purpose (Figure 4.1).

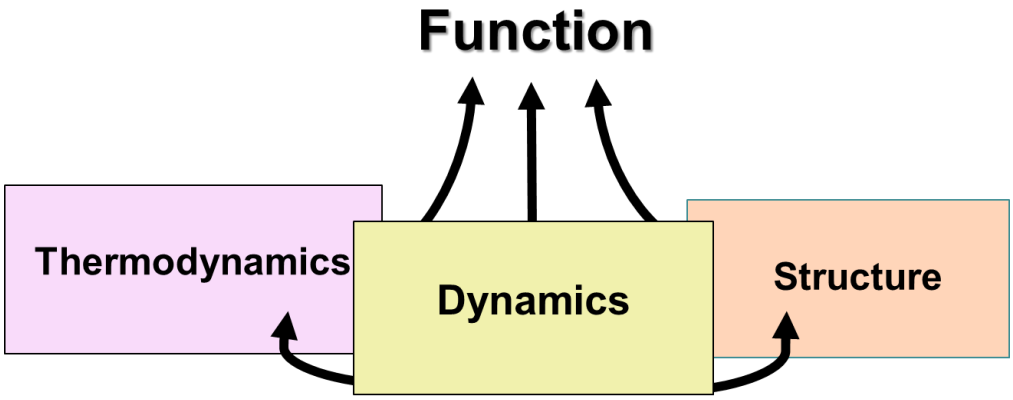

Figure 4.1. Schematic representation of the connection between supramolecular systems' structure, thermodynamics, and dynamics.

Understanding the thermodynamics of supramolecular systems provides information about their structure, and vice versa. However, neither thermodynamics nor structure alone cannot explain the mechanisms of these systems. The mechanism by which a supramolecular system achieves its function, remains a gap in knowledge in this field. To understand the mechanism, the dynamics of these systems must be studied. By investigating the dynamics and mechanisms, researchers can gain a deeper understanding of how supramolecular systems function. This understanding can then be used to design and control the thermodynamic state and structure of supramolecular systems. Hence, understanding the mechanism of these systems requires studying their kinetics.

Introducing new components to supramolecular hydrogels can significantly change their kinetics. For example, adding a secondary host molecule like CB[7] alongside the primary host (NaDC) can change the binding kinetics of small molecules. CB[7] can form complexes with both NaDC and guest molecules, leading to competitive binding. This competition affects the rates of association and dissociation and changes the overall kinetics of the system.

The primary focus of this study was to study how the host-guest interactions of CB[7] affect the properties of the NaDC supramolecular hydrogel. To achieve this goal, several approaches were taken, and each was focusing on a different dimension of the NaDC hydrogel. First of all, the structure of the NaDC hydrogel was monitored after the addition of CB[7]. Secondly, the effect of NaDC aggregates on the dissociation of the guest molecule (berberine) from CB[7] was studied as part of the mechanistic analysis in solution. Lastly, release kinetic studies were conducted to analyze the release of a guest molecule (rhodamine 6G) from the NaDC hydrogel in the presence of CB[7]. These studies were done to compare the addition of CB[6] in the NaDC hydrogel, as previously done by the Bohne group. CB[6] and CB[7] have structural differences, and it is expected that they would localize differently within the NaDC hydrogel.

It has been observed that CB[7] has less effect on the length of NaDC immobilized aggregates, although it does not induce a fibrous structure in the gel network as CB[6] does. Additionally, the incorporation of CB[7] into the NaDC hydrogel is more constrained compared to CB[6]. This difference in behavior can be attributed to CB[7]'s higher solubility in water and its lower tendency to integrate into the gel structure compared to CB[6]. The steady-state

fluorescence and UV-Vis absorption studies suggested that positively charged guests like berberine might not exclusively form complexes with CB[7] due to the negative charges of the NaDC aggregates. Positive charge of berberine lead to a distribution of berberine between complexation with CB[7] and interaction with NaDC aggregates. Kinetic studies showed that the presence of NaDC aggregates changes the dissociation rate constant of berberine from CB[7]. This change in the dissociation rate constant of berberine from CB[7] may be attributed to the relocation of the berberine complexed with CB[7] from bulk water to the NaDC aggregates. Additionally, the higher probability of the presence of positively charged Ada^+ in the negatively charged aggregates could contribute to this effect. Release studies have also shown the interaction between the positive charge of the guest (rhodamine 6G) and negative charges of the NaDC aggregates as there is no change in the release upon the addition of CB[6] or CB[7]. For future studies, it is suggested to use a hydrophobic and neutral guest.This approach eliminates charge interactions between the NaDC aggregates and the dye, potentially providing clearer insights between the effect of CB[6] and CB[7] interaction on the release of the guest.

Appendix

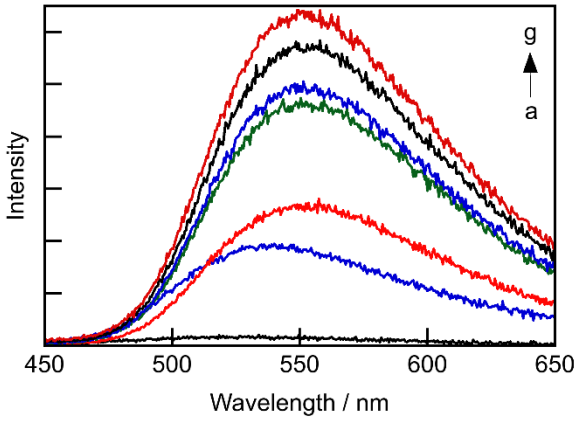

Figure A2.1. Steady-state fluorescence emission spectra of 10 μM berberine (λ_{ex} = 345 nm) with 1 (a, lower black), 5 (b, lower blue), 10 (c, lower red), 15 (d, green), 20 (e, upper blue), 30 (f, upper black), 50 mM (upper red) (a → g) NaDC.

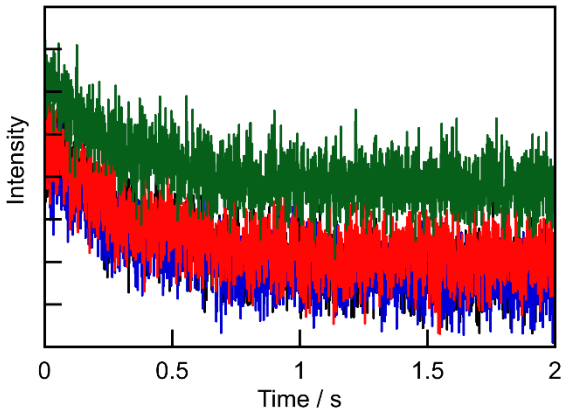

Figure A2.2. Stopped-flow kinetic traces for the mixing of a solution containing of 0.25 μM berberine with 0.75 μM CB[7] and 25 mM NaDC with 2 (black), 5 (lower blue), 10 (red), 20 (lower green), 40 (black), 80 μM (upper green) Ada^+ ($[Na^+]$ = 50 mM). All the concentrations mentioned are after mixing. All traces except the green trace are overlapping.

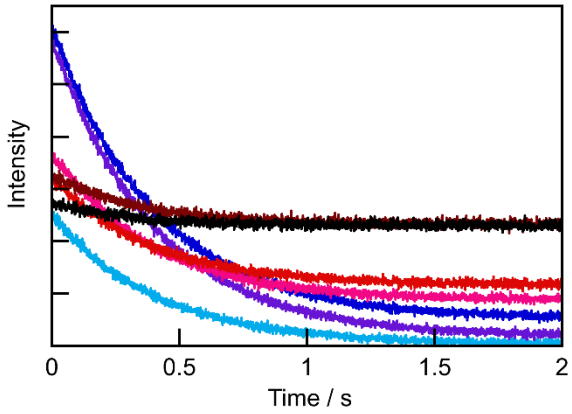

Figure A2.3. Stopped-flow kinetic traces for the mixing of 5 μM Ada^+ with solutions containing 0.25 μM berberine, 0.75 μM CB[7] and different concentrations of NaDC. Lower concentrations of NaDC (0, 0.5, 2 mM) are shown as a blue gradient from light blue to purple and higher concentrations (5, 6, 15, 25 mM) are shown as a red gradient from pink to black) ($[Na^+]$ = 50 mM). All the concentrations mentioned are after mixing.

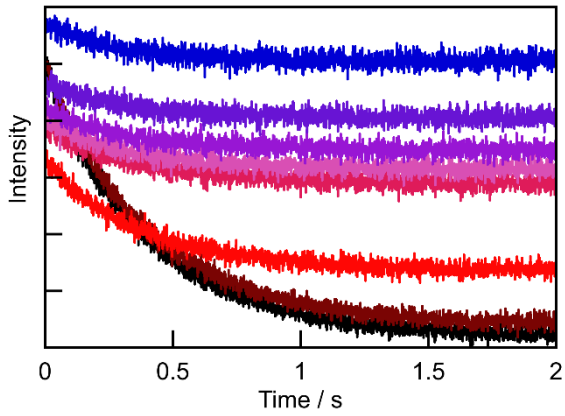

Figure A2.4. Stopped-flow kinetic traces for the mixing 40 μM Ada^+ with solutions containing 0.25 μM berberine, 0.75 μM CB[7] and different concentrations of NaDC. Low concentrations of NaDC (0, 2, 5, 10, 12 mM) are shown as a red gradient from black to light pink and higher concentrations (15, 20, 25 mM) are shown as a blue gradient from light purple to blue ($[Na^+]$ = 50 mM). All the concentrations mentioned are for after mixing.